



Spatial linkages between coral proxies of terrestrial runoff across a large embayment in Madagascar

C. A. Grove¹, J. Zinke^{1,2}, T. Scheufen^{1,3,*}, J. Maina⁴, E. Epping¹, W. Boer¹, B. Randriamanantsoa⁵, and G.-J. A. Brummer¹

¹Department of Marine Geology, Royal Netherlands Institute for Sea Research (NIOZ), P.O. Box 59, 1790 AB Den Burg, Texel, The Netherlands

²School of Earth and Environment, The University of Western Australia and the UWA Oceans Institute, 35 Stirling Highway, Crawley WA 6009, Australia and the Australian Institute of Marine Science, 39 Fairway, Nedlands WA 6009, Australia

³University of Amsterdam, Institute for Biodiversity and Ecosystem Dynamics (IBED), Nieuwe Achtergracht 127, 1018 WS Amsterdam, The Netherlands

⁴Department of Biological Sciences, Macquarie University, Sydney NSW, Australia

⁵Wildlife Conservation Society (WCS), B. P. 8500 Soavimbahoaka, Antananarivo 101, Madagascar

* now at: Unidad Académica de Sistemas Arrecifales, Instituto de Ciencias del Mar y Limnología, Universidad Nacional Autónoma de México, Apdo. Postal 1152, Cancún, Quintana Roo 77500, Mexico

Correspondence to: C. A. Grove (craig.grove@nioz.nl)

Received: 27 February 2012 – Published in Biogeosciences Discuss.: 14 March 2012

Revised: 5 July 2012 – Accepted: 17 July 2012 – Published: 10 August 2012

Abstract. Coral cores provide vital climate reconstructions for site-specific temporal variability in river flow and sediment load. Yet, their ability to record spatial differences across multiple catchments is relatively unknown. Here, we investigate spatial linkages between four coral proxies of terrestrial runoff and their relationships between sites. Coral cores were drilled in and around Antongil Bay, the largest bay in Madagascar, and individually analysed for fifteen years of continuous luminescence (G/B), Ba/Ca, $\delta^{18}\text{O}_{\text{sw}}$ and $\delta^{13}\text{C}$ data. Each coral core was drilled close to individual river mouths (≤ 7 km), and proxy data were compared to modelled river discharge and sediment runoff data for the three corresponding catchments. A reasonable agreement between terrestrial runoff proxies with modelled river discharge and sediment yield was observed. Some inconsistencies between proxy and modelled data are likely linked to proxy behaviour, watershed size and local environmental physiochemical parameters. In general, the further a coral resided from its river source, the weaker the proxy relationship was with modelled data and other corals, due to mixing gradients and currents. Nevertheless, we demonstrate that two coral Ba/Ca and luminescence (G/B) records influenced by the same watershed are reproducible. Furthermore, a strong

Ba/Ca relationship was observed between two cores from distant watersheds, with baseline averages in agreement with modelled sediment runoff data. As humic acids behave conservatively in the water column, luminescence (G/B) data gave the highest regional correlations between cores, and showed the most consistent relationship with site specific modelled discharge. No statistical relationship was observed between cores in terms of interannual $\delta^{18}\text{O}_{\text{sw}}$ and $\delta^{13}\text{C}$, meaning corals were recording a localised signal at their respective sites, confounded by vital effects. Comparing proxy baseline averages and mean seasonal cycles provided a good overview of the runoff dynamics of the bay system.

1 Introduction

Anthropogenic and climate-induced changes in sediment load entering the coastal realm are of great concern for the sustainability of tropical marine and terrestrial environments (Rogers, 1990; McClanahan and Obura, 1997; McCulloch et al., 2003; Payet and Obura, 2004). Deforestation often leaves soils susceptible to erosion (Green and Sussman, 1990; Agarwal et al., 2005) thus altering the amount and characteristics

of both sediment and leached dissolved components delivered to the coastal ocean (Warrick and Rubin, 2007). Madagascar is an iconic example of the extreme environmental impacts human deforestation and habitat destruction has on soil runoff and land degradation (Green and Sussman, 1990; Harper et al., 2007). It is now estimated that only 10–15% of the original forests remain since extensive deforestation began in the mid 20th century (Green and Sussman, 1990; Harper et al., 2007). Forest protection and management can help stabilise soils within catchment areas, yet requires continuous records of site specific land-use changes, erosion and weather patterns to differentiate between vulnerable and stable areas.

In Madagascar, weather station data are scarce (Dewar and Wallis, 1999; Dewar and Richard, 2007) and satellite derived rainfall data around coastal regions with high cloud cover are often unreliable (Quartly et al., 2007). Previous research efforts in Madagascar have focussed on terrestrial environments, yet an assessment of the status of the coastal marine ecosystems in relation to climatic and anthropogenic stressors is lacking (Goodman and Benstead, 2003; Kremen, 2003). Proxy climate and environmental records preserved in annually-banded massive corals, such as *Porites* spp., can significantly augment the instrumental data that are often too short to identify change in many tropical regions. Massive corals can grow for centuries at relatively fast rates (1–2 cm yr⁻¹), incorporating trace elements (TE) into the aragonite skeleton according to their relative concentrations in ambient sea water during calcification (Alibert et al., 2003; McCulloch et al., 2003; Lewis et al., 2007; Jupiter et al., 2008; Jones et al., 2009). Such properties make massive corals ideal archives of localised environmental change (e.g. river discharge, sediment load). The down-core analyses of coral proxies in long coral cores can provide information on site-specific temporal variability in river flow and sediment loads influencing corals. Such information can potentially assist in the management of watersheds in Madagascar where instrumental data on water characteristics are lacking. However, the reliability of coral proxies is still debated as cores from the same region can often show varying signals (Jones et al., 2009; Pfeiffer et al., 2009; Lewis et al., 2011).

Luminescence of the coral skeleton is used as a tracer of temporal variability in river flow. First described by Isdale (1984), the intensity of luminescent lines in corals was thought to be caused by the skeletal incorporation of humic acids (HA) derived from hinterland soils. Subsequent reports indicated that luminescence may also result from changing skeletal densities (Barnes and Taylor, 2001, 2005). More recently, spectral luminescence scanning (SLS) has shown that both processes contribute to luminescence and that humic acids can be normalised for the effects of changing skeletal density to provide an indicator of humic acid runoff (Grove et al., 2010). As the luminescent emission signal of HA is slightly longer than aragonite, taking the green/blue (G/B) ratio gives an estimate of the amount of HA relative to the

skeletal density (Grove et al., 2010). SLS resolves density effects associated with luminescence intensities, such as declining trends in intensity with coral age (Lough, 2011a, b; Jones et al., 2009).

Barium (Ba) is both dissolved in the rivers and adsorbed to suspended sediments (clay minerals), which are then transported to coastal waters via rivers. As salinities increase, Ba desorbs from the suspended sediment due to the higher ionic strength of seawater. As Ba is diluted by seawater it is thought to follow a conservative mixing pattern (Sinclair and McCulloch, 2004), and thus Ba acts as a tracer for riverine sediment input to the coastal ocean. As Ba substitutes Ca in the coral skeleton, sediment discharge is reconstructed accordingly using skeletal Ba/Ca ratios (Sinclair and McCulloch, 2004; Alibert et al., 2003; McCulloch et al., 2003; Fleitmann et al., 2007). However, as estuarine processes, such as phytoplankton uptake and resuspension, can lead to a non-conservative behaviour of Ba (Hanor and Chan, 1977; Coffey et al., 1997); subsequently, sediment discharge reconstructions can be affected (Sinclair, 2005). In such circumstances, skeletal Ba/Ca levels may not be directly related to sediment discharge.

Coral skeletal $\delta^{18}\text{O}$ is a function of both SST and salinity. Calculating the difference between coralline $\delta^{18}\text{O}$ and the sea surface temperature proxy Sr/Ca provides a salinity proxy, $\delta^{18}\text{O}_{\text{seawater}}$ ($\delta^{18}\text{O}_{\text{sw}}$) (Sinclair and McCulloch, 2004; McCulloch et al., 1994, 2003). Indeed, here we couple $\delta^{18}\text{O}$ and Sr/Ca following the method of Ren et al. (2002) to reconstruct the $\delta^{18}\text{O}$ of seawater ($\delta^{18}\text{O}_{\text{sw}}$). Potentially, $\delta^{18}\text{O}_{\text{sw}}$ can identify the coral experiencing the lowest and highest salinities. This in turn can enhance our interpretation of the other runoff proxies by factoring in mixing processes.

The Sr/Ca ratio of the coral aragonite seems to be the most robust paleo-thermometer, whereby a negative relationship exists with SST, i.e. as temperatures increase, less Sr is incorporated into the aragonite lattice relative to Ca (Alibert and McCulloch, 1997; DeLong et al., 2007). However, recently published coral Sr/Ca records covering the past hundreds of years indicate specific problems with the Sr/Ca thermometer, particularly on decadal to secular time scales (e.g. Linsley et al., 2004, 2006; Quinn et al. 2006). Pfeiffer et al. (2009) showed that the intrinsic variance of the single-core Sr/Ca time series differs from core to core, limiting their use for absolute estimates of past temperature variations. This inter-colony variability seems linked to vital effects.

The stable isotopes $\delta^{18}\text{O}$ and $\delta^{13}\text{C}$ are known to be affected by vital effects, i.e. kinetic effects, light, pH variation at sites of calcification, skeletal architecture and the influence of metabolic CO_2 etc. (McConnaughey, 2003; Felis et al., 2003; Rollion-Bard et al., 2003). Coral skeletal $\delta^{13}\text{C}$ is linked to runoff processes, including the $\delta^{13}\text{C}$ composition of DIC and reduction of light associated with river plumes. However, as $\delta^{13}\text{C}$ is confounded by many vital effects it is difficult to interpret (Grottolli, 2002; McConnaughey, 2003;

Grottoli and Wellington, 1999; Swart et al., 1996; Reynaud-Vaganay et al., 2001; Reynaud et al., 2002).

The DIC of riverine waters is typically more isotopically depleted than seawater $\delta^{13}\text{C}$, caused by the decay of strongly depleted terrestrial vegetation (Moyer, 2008; von Fischer and Tieszen, 1995; Moyer and Grottoli, 2011; Marin-Spiotta et al., 2008). The input of riverine DIC to the coastal ocean will therefore cause depletions in the $\delta^{13}\text{C}$ of ambient seawater DIC and coral skeletons. A reduction in incident light levels may also play a role in determining the skeletal $\delta^{13}\text{C}$ variability (Grottoli, 2002; Grottoli and Wellington, 1999). As sediment and humic acid concentrations increase with runoff, turbidity reduces the incident light reaching benthic communities, including the corals (Larsen and Web, 2009). During photosynthesis the endosymbiotic algae (*Symbiodinium* sp.) preferentially utilise ^{12}C for biomass production, leaving the carbon pool, used by the coral for calcification, enriched in ^{13}C (Weil et al., 1981; Swart et al., 1996; Reynaud-Vaganay et al., 2001; Reynaud et al., 2002). Reduced photosynthesis will reduce the depletion of ^{12}C in the carbon pool and thus the skeletal material will have a lighter $\delta^{13}\text{C}$, yielding an inverse relationship with increasing runoff.

In this study, we collected four coral cores from *Porites* colonies across three watersheds surrounding Antongil Bay in eastern Madagascar. We first examine the reproducibility of the common river runoff proxies Ba/Ca and Luminescence (G/B) for two corals associated with the largest watershed. Secondly, we examine the relationships of four coral proxies indicating river flow, sediment load, salinity and turbidity/DIC (luminescence (G/B), Ba/Ca, $\delta^{18}\text{O}_{\text{sw}}$, $\delta^{13}\text{C}$) for coral cores located in the same region, yet associated with three separate river systems. We test whether individual proxies reflect a regional river runoff signal, a localised signal or a combination of both. As the temporal variation of river discharge recorded by corals is a function of the distance from a river source (salinity gradient) and the flow direction, as well as the source input, comparing rivers using corals from different reefs is challenging (King et al., 2001; Lough et al., 2002; Carricart-Ganivet et al., 2007; Jupiter et al., 2008; Prouty et al., 2010). To test how representative proxies are of their corresponding river watersheds, we combine coral proxies and compare results with modelled river discharge and sediment yield.

2 Materials and methods

2.1 Research area and climate setting

Antongil Bay is located in the NE of Madagascar (Fig. 1) covering an area of 2800 km², with a mean depth of 41.5 m and a coastline of 270 km extending 80 km inland (Ersts and Rosenbaum, 2003). Almost all populated areas are located in the northern and western coastal regions of the bay, including the largest urban areas of Maroantsetra and Mana-

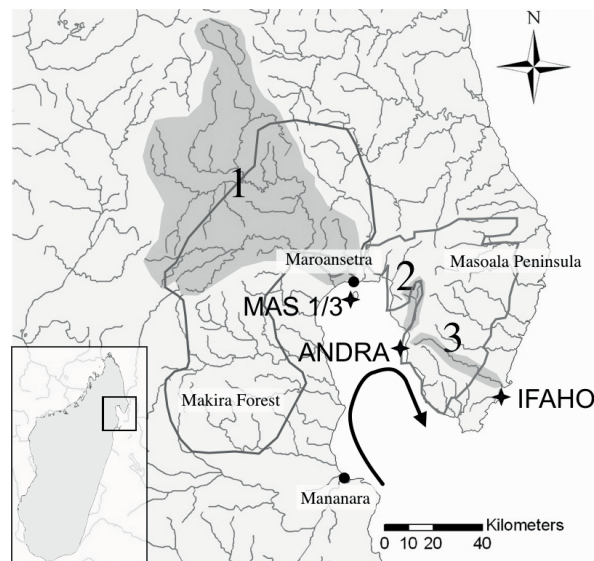


Fig. 1. Map of Antongil Bay in NE Madagascar showing the three coral sites (stars) and closest rivers with respective watersheds (grey shaded areas). Rivers are marked by the numbers 1 (MAS1, Antainambalana River), 2 (ANDRA, Ambanizana River) and 3 (IFAHO, Anaovandran River). The bay circulation is marked by an arrow indicating a clockwise direction. The location of towns (black circles) and national park boundaries (Makira-Masoala Protected Landscape; thick grey lines) are marked on the map accordingly.

nara. Two protected forest areas are found in the vicinity of the bay, the Makira Forest and the Masoala Peninsula National Park. The Makira Forest extends over 4600 km² north of Maroantsetra, and together with the Masoala Peninsula National Park forms one of the largest continuous rain-forest areas remaining in Madagascar (Birkinshaw and Randrianjanahary, 2007). Since the introduction of the National Park there has been a significant reduction in the rate of deforestation, yet it still remains a constant threat to the marine and terrestrial environments (Harper et al., 2007).

One of the largest rivers draining into Antongil Bay is the Antainambalana, running through the Makira Forest Area from a source 1450 m above sea level (Goodman and Ganzhorn, 2004). Its watershed covers an estimated 4000 km² and the river mouth is located in the city of Maroantsetra (Fig. 1 and Table 1). The coral cores MAS1 and MAS3 were collected 40 m apart next to the island Nosy Mangabe, ca. 7 km from the river mouth, on the edge of a fringing reef slope and reef flat, respectively, at approximately 4 m water depth (Fig. 1 and Table 1). The ANDRA coral core was collected 30 km from MAS1 from the fringing reef slope on the east side of the bay, ca. 7 km from the Ambanizana river mouth, at 4 m water depth (Fig. 1 and Table 1). The Ambanizana has a much smaller watershed

Table 1. Coral cores with GPS co-ordinates, growth rates, total core length, distance and name to the closest river source.

Coral core	Location	Distance to closest river source (km)	Average growth rate (mm yr ⁻¹)	Core length (cm)
MAS1	S 15°30.566 E 49°45.437	7 Antainambalana	11.8	121
MAS3	S 15°30.578 E 49°45.456	7 Antainambalana	11.1	143
ANDRA	S 15°41.17 E 49°57.419	7 Ambanizana	12.7	120
IFAHO	S 15°51.968 E 50°18.73	4.5 Anaovandran	14.1	38

(ca. 160 km²) and runs southwest towards Antongil Bay through a mountainous region with dense forest cover. Both the Ambanizana and the Antainambalana drain a hinterland that mainly consists of granitic soils (Collins, 2006; Kremen et al., 1999). The IFAHO coral is situated ca. 4.5 km from the mouth of the river Anaovandran (watershed: ca. 180 km²) outside of Antongil Bay (Fig. 1 and Table 1). The river originates from the same mountains as the Ambanizana, but flows eastwards away from Antongil Bay. For the last ca. 11 km it runs through a plain before entering the ocean (Windley et al., 1994 and references therein). The Anaovandran drains a hinterland that consists of granitic soils at high elevations and basaltic rocks that cover the lower elevation partly deforested sedimentary plain (Douglas, 1967; Collins, 2006; Kremen et al., 1999). The IFAHO coral core was drilled at 6 m water depth and collected from the back reef of a fringing reef where direct influence of the open ocean is restricted.

The climate in Madagascar can be divided into a August–December cold-dry season and a January–July warm-wet season (Fig. 2). Air temperatures peak in December and January and are lowest between July and September (Kremen, 2003). The sea surface temperature (SST) peaks between December and April, reaching maximum average temperatures of 28.7 °C (Fig. 2). Minimum average SST are 24.6 °C, meaning there is a mean seasonal range of 4.1 °C. Highest rainfall occurs between January and March, while lowest rainfall occurs between September and November (Xie and Arkin, 1996). Average rainfall levels reach 300 mm month⁻¹ during the wet season (January to March) and 50 mm month⁻¹ in the dry season. Average peak river discharge occurs between January and April. River discharge then decreases yet continues all year round, reaching lows in October and November (Fig. 2).

2.2 Coral sampling

Coral cores were drilled from massive colonies of *Porites* spp. at depths between 4–6 m at different locations in and around Antongil Bay, NE Madagascar (Fig. 1 and Table 1) during March and April 2007. A commercially available pneumatic drill (Rodcraft 4500) was used to extract 4 cm

diameter cores along the central growth axis of the colony. In contrast to the results of Matson (2011), drill holes were not plugged as algal growth was observed on the concrete plugs from earlier drilling campaigns. Drill holes closed by natural coral growth within 2 yr when left. Cores were sectioned lengthwise into 7 mm thick slabs, rinsed several times with demineralised water, blown with compressed air to remove any surficial particles and dried for more than 24 h in a laminar flow hood. Annual density bands were visualised by X-radiograph-positive prints, and the growth axis of the coral slab was defined as the line perpendicular to these bands. The average growth rate of all four coral cores was approximately 13 ± 2 mm y⁻¹ (Grove et al., 2010 and Table 1). With a diamond coated drill, subsamples were taken every 1 mm parallel to the growth axis, equivalent to approximately monthly resolution. All coral slabs were cleaned with sodium hypochlorite (NaOCl, 10–13 % reactive chloride; Sigma-Aldrich Company) for 24 h, after sub-sampling for geochemistry, to remove residual organics that might quench luminescence (Nagtegaal et al., 2012).

2.3 Coral luminescence

SLS was performed, as described by Grove et al. (2010), on bleached coral slabs using a line-scan camera fitted with a Dichroic beam splitter prism, separating light emission intensities into three spectral ranges; blue (B), green (G) and red (R). The four coral cores used for this study were also analysed in the study of Grove et al. (2010) to test the performance of the SLS technique. Digital core images were analysed with the Line Scan Software Version 1.6 (Avaatech), providing RGB intensity values for individual pixels of 71 µm in length. Since the spectral emissions of humic acids are slightly longer than aragonite, spectral G/B ratios reflect the changing humic acid/aragonite ratios within the coral skeleton (Grove et al., 2010). The G/B datasets for the four corals applied in this study all begin in January 1991 and end in December 2005, spanning a total of 15 yr.

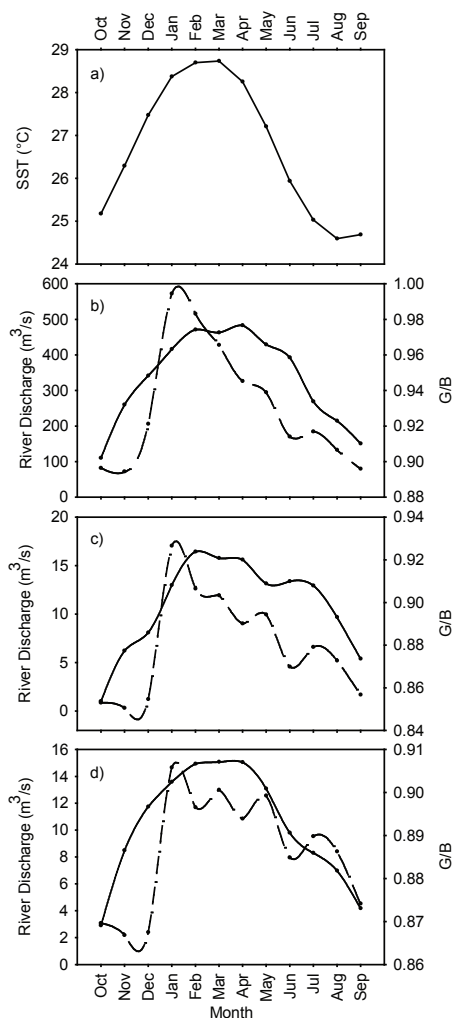


Fig. 2. Average seasonal cycle of SST (a) (ERSST; Smith et al., 2008) for Antongil Bay (52° E, 16° S) calculated by averaging every month over a 15 yr period (1991–2005). Similarly, over the same 15 yr period, the average seasonal G/B (solid line) and modelled river discharge data (dashed line) are calculated for the corals (b) MAS1, (c) ANDRA and (d) IFAHO and their closest respective rivers (b) the Antainambalana River, (c) the Ambanizana River and (d) the Anaovandran River.

2.4 Coral geochemistry

Two measurement techniques, solution ICP-MS and LA-ICP-MS, were applied to compare Ba/Ca data generated for two coral cores, MAS1 and MAS3 (LA-ICP-MS only), from the same catchment. Both time series begin in January 1991 and end in December 2005, spanning a total of 15 yr. Solution ICP-MS was also applied to generate both Ba/Ca and Sr/Ca data for the cores MAS1, ANDRA and IFAHO for the same 15 yr period, at an approximate monthly resolution. Subsamples were taken every 1 mm equating to ca. 1 month resolution. This is in contrast to the approximate sub-weekly

resolution of the LA-ICP-MS technique. Stable isotope data were generated for the same three corals measured using solution ICP-MS (MAS1, ANDRA and IFAHO), at the same ca. monthly resolution (subsample resolution).

2.4.1 Solution ICP-MS

Sr/Ca and Ba/Ca were analysed for MAS1, ANDRA and IFAHO by high resolution inductively coupled plasma mass spectrometry (HR-ICP-MS; Thermo Scientific Element-2) equipped with a double spray chamber and Teflon microflow nebulizer. The method of sample dissolution, dilution, quantification, and drift correction is described in Nagtegaal et al. (2012). Accuracies were determined using a JCp-1 *Porites* sp. coral standard. Accuracies for Sr/Ca were $99.8 \pm 0.5\%$ ($8.80 \text{ mmol mol}^{-1}$) and for Ba/Ca $97 \pm 6\%$ ($7.16 \text{ } \mu\text{mol mol}^{-1}$). Short-term (< 5 min) precision and longer-term precision (8 batches measured during 1 month) were typically 0.2% and 0.5% RSD for Sr/Ca, respectively, and 0.2% and 6% for Ba/Ca. Short-term precision reflects variability in operating conditions such as power and gas flow rates. Longer-term stability mainly reflects the goodness of drift corrections. Blanks were kept low using ultrapure acids. Blanks were always < 0.5% for Sr/Ca and < 2% for Ba/Ca.

2.4.2 LA-ICP-MS

Laser ablation inductively coupled mass spectrometry (LA-ICP-MS) analytical methods were identical to those reported in Jupiter et al. (2008). The coral slabs of cores MAS1 and MAS3 were mounted on a stage containing standards and analysed using a Varian 820 inductively coupled mass spectrometer. The laser slit size was $40 \times 400 \text{ } \mu\text{m}$, yielding a sampling resolution of 20 nm. The resultant data were normalised to ^{43}Ca using a Varian laser scanning analysis software program developed at the Australian National University (ANU) Research School of Earth Sciences (by L. Kinsley). Data were first smoothed using a 10 point running mean to reduce the influence of outliers, followed by a 10 point mean to reduce data volume. To determine accuracy, a NIST 614 glass standard and a pressed coral standard were used (Fallon et al., 1999, 2002). The overall analytical precision for Ba/Ca was 4.3% (Fallon et al., 1999). Daily and long-term (5 month) reproducibility was monitored by repeated measurements of the pressed coral standard and an in-house coralline sponge standard (Fallon et al., 1999). The daily and long-term reproducibility was 1.6% and 3.3%, respectively. The analytical internal precision for Ba/Ca was < 4.3% RSD (Fallon et al., 1999). Further details on the methodology and standards are available in Fallon et al. (1999, 2002). The Ba/Ca (LA-ICP-MS) datasets for the two corals MAS1 and MAS3 begin in January 1991 and end in December 2005, spanning a total of 15 yr.

2.4.3 Stable isotopes

To measure the skeletal $\delta^{18}\text{O}$ and $\delta^{13}\text{C}$, approximately 80 μg of coral powder was reacted with H_3PO_4 in an automated carbonate reaction device (Kiel IV) connected to a Finnigan MAT 253 mass spectrometer at the Royal Netherlands Institute for Sea Research (NIOZ). For the NBS19 carbonate standard (standard values are -2.2‰ and 1.95‰ for $\delta^{18}\text{O}$ and $\delta^{13}\text{C}$, respectively) we obtained values of $-2.21 \pm 0.08\text{‰}$ and $1.96 \pm 0.04\text{‰}$ for $\delta^{18}\text{O}$ and $\delta^{13}\text{C}$, respectively, relative to the Vienna PeeDee Belemnite (V-PDB) standard. Solution ICP-MS Ba/Ca, Sr/Ca and the stable isotope datasets for the three corals MAS1, ANDRA and IFAHO all begin in January 1991 and end in December 2005, spanning a total of 15 yr.

2.4.4 Reconstructing salinity

To calculate $\delta^{18}\text{O}_{\text{seawater}}$ ($\delta^{18}\text{O}_{\text{sw}}$), we followed the method of Ren et al. (2002). The method assumes that coral Sr/Ca is solely a function of SST and that coral $\delta^{18}\text{O}$ is a function of both SST and $\delta^{18}\text{O}_{\text{sw}}$. This method separates the effects of $\delta^{18}\text{O}_{\text{sw}}$ from SST by breaking the instantaneous changes of coral $\delta^{18}\text{O}$ into separate contributions by instantaneous SST and $\delta^{18}\text{O}$ changes, respectively. We used the $\delta^{18}\text{O}_{\text{coral}}\text{-SST}$ relationship of $-0.2\text{‰}\text{ }^\circ\text{C}$ (Juilliet-Leclerc and Schmidt, 2001) and the Sr/Ca-SST relationship of $-0.06\text{ mmol mol}^{-1}\text{ }^\circ\text{C}$ (Corrège, 2006) to calculate the instantaneous changes in SST. Taking into account the uncertainties associated with the analytical precision of (1) coral $\delta^{18}\text{O}$, (2) coral Sr/Ca, (3) the coral Sr/Ca-SST calibration and (4) the coral $\delta^{18}\text{O}\text{-SST}$ calibration, we calculated a monthly $\delta^{18}\text{O}_{\text{sw}}$ error of 0.09 ‰ (following Zinke et al., 2008). Based on the local salinity- $\delta^{18}\text{O}_{\text{sw}}$ relationship for Antongil bay, the error in reconstructed salinity equates to 0.67 psu for monthly values and 0.19 psu for mean annual values (Sect. 2.7).

2.5 Hydrological modelling

Due to a lack of hydrological data for Madagascar we used model results of river discharge and sediment yield in the Antongil Bay (Maina et al., 2012). Maina et al. (2012) used the STREAM (Spatial Tools for River basins, Environment and Analysis of Management options) grid-based hydrological model to simulate monthly river discharge (Aerts and Bouwer, 2002; Aerts et al., 1999). STREAM simulates the water balance for each grid (50 km resolution) using a limited number of parameters, including spatial-temporal precipitation and temperature trends, elevation, land-cover and soil water storage capacity specific to Madagascar (Aerts and Bouwer, 2002). The STREAM model has been successfully applied in various climate and hydrological studies (e.g. Bouwer et al., 2006; Winsemius et al., 2006), which have shown that a monthly time step is sufficient for detecting decadal, inter-annual and seasonal hydrological cycles.

Here, we extracted the average seasonal cycle in river discharge for the three rivers studied and the average yearly river discharge per catchment (Maina et al., 2012).

Sediment yield per unit area was computed using the Non-Point Source Pollution and Erosion Comparison Tool (N-SPECT) developed by the National Oceanic and Atmospheric Administration (NOAA) (<http://www.csc.noaa.gov/digitalcoast/tools/nspect/index.html>). N-SPECT combines data on elevation, slope, soils, precipitation, and land cover to derive estimates of runoff, erosion, and pollutant sources (nitrogen, phosphorus, and suspended solids) from across the landscape, as well as estimates of sediment and pollutant accumulation in stream and river networks. Erosion rates and sediment loads were calculated using the Revised Universal Soil Loss Equation (RUSLE) and Modified Universal Soil Loss Equation (MUSLE) (Wischmeier and Smith, 1978). N-SPECT provides annual mean (January–December) estimates of sediment yield per unit area in mt yr^{-1} at a 50 km resolution. Here, we extracted the average yearly river sediment yield per catchment (Maina et al., 2012).

2.6 Coral age model construction

Coral chronologies were based on the seasonal cycle of Ba/Ca and G/B ratios. Luminescence in corals has previously been used to cross date core records (Hendy et al., 2003; Grove et al., 2010) and assist in establishing a chronology for growth and geochemical tracers (Smithers and Woodroffe, 2001; Cole et al., 2000; Fleitmann et al., 2007). In Antongil Bay, the driest month on average in a given year is October (Kremen, 2003). Consequently Ba/Ca and G/B minima were assigned to October (Fig. 2), creating consistent age models for all cores. All years were then interpolated linearly between the October anchor points using AnalySeries 2.0 (Paillard et al., 1996). This resulted in a time scale of monthly resolution with 12 equidistant data points. Annual anomalies were calculated by averaging all monthly values between January and December for any given year. This gave the best fit between cores, and allowed for direct comparison with modelled sediment yield data. Linear correlations between proxy data were computed using the software “R”.

The mean seasonal cycle of Ba/Ca, G/B, $\delta^{18}\text{O}_{\text{sw}}$ and $\delta^{13}\text{C}$ for each core were constructed by calculating the monthly mean over the 15 yr record length. Comparing the mean seasonal cycle of G/B with the mean seasonal cycle of modelled river discharge for each of the three individual watersheds indicates that there is good agreement between the two data in terms of temporal alignment (Fig. 2). This gives us confidence in our age model for each of the coral core records.

Table 2. Correlation coefficients of seasonal (upper) and annual average (lower) coral proxy data between the three coral sites MAS1, ANDRA and IFAHO, and LA-ICP-MS data for MAS1 and MAS3. Significance levels are given in parentheses, and correlation coefficients, which are below the significance level of $P < 0.05$, are marked with a star (*). The annual average proxy values were calculated by averaging the months January to December for which the highest between core correlations were found.

Proxy	MAS1 vs. MAS3	MAS1 vs. ANDRA	MAS1 vs. IFAHO	ANDRA vs. IFAHO
G/B	0.74 ($P < 0.001$)*	0.67 ($P < 0.001$)*	0.66 ($P < 0.001$)*	0.56 ($P < 0.001$)*
Ba/Ca	0.71 ($P < 0.001$)*	0.071 ($P = 0.35$)	0.49 ($P < 0.001$)*	0.095 ($P = 0.21$)
$\delta^{18}\text{O}_{\text{sw}}$	–	0.12 ($P = 0.11$)	0.17 ($P = 0.022$)*	0.046 ($P = 0.54$)
$\delta^{13}\text{C}$	–	0.0052 ($P = 0.94$)	0.097 ($P = 0.19$)	0.052 ($P = 0.49$)
G/B	0.67 ($P = 0.007$)*	0.69 ($P = 0.005$)*	0.50 ($P = 0.056$)	0.63 ($P = 0.013$)*
Ba/Ca	0.88 ($P < 0.001$)*	0.37 ($P = 0.17$)	0.66 ($P = 0.008$)*	0.27 ($P = 0.32$)
$\delta^{18}\text{O}_{\text{sw}}$	–	0.28 ($P = 0.32$)	0.41 ($P = 0.13$)	0.014 ($P = 0.96$)
$\delta^{13}\text{C}$	–	0.12 ($P = 0.68$)	0.15 ($P = 0.60$)	0.32 ($P = 0.25$)

2.7 Seawater analyses

We established the local salinity- $\delta^{18}\text{O}$ relationship from a set of water samples to subsequently reconstruct salinity from coral skeletal $\delta^{18}\text{O}_{\text{sw}}$, as derived from coupled coral Sr/Ca and $\delta^{18}\text{O}$ measurements (Ren et al., 2002). We obtained the seawater $\delta^{18}\text{O}$ and salinity for seven water samples collected in October 2008, representing the dry season, and a further sample taken in March 2007, capturing the wet season signal. The seven samples were collected along an inshore-offshore gradient between the mouth of the river Antainambalana and the MAS1 coral. The salinity of each water sample, taken in pre-cleaned 1 litre HDPE bottles, was measured with a handheld probe (Vernier) and a fraction was stored in air-tight 100 ml glass bottles. All water samples were subsequently poisoned with HgCl_2 to prevent biological activity. Samples were then analysed for $\delta^{18}\text{O}$ on a Thermo Finnigan Delta+ mass spectrometer equipped with a GASBENCH-II preparation device at the VU Amsterdam. A 0.5–1 ml water sample was injected through the septum cap of a 10 ml exetainer vial filled with a mixture of He and 0.2% CO_2 to equilibrate with the oxygen in the headspace CO_2 for 24 h at 22 °C. Subsequently, the headspace mixture is transported by a He carrier flow (dehydrated using NAFION tubing) for analysis of CO_2 in the mass spectrometer after gas separation in a GC column. Values are reported as $\delta^{18}\text{O}$ vs. V-SMOW with a long-term reproducibility better than 0.1‰ (1SD) for a routinely analysed lab water standard.

3 Results

The results section begins with a comparison of Ba/Ca and G/B variability between cores from a single site to assess proxy reproducibility. Next, we compare the variability of four proxies at three different locations to assess regional similarities. This section also includes a detailed description

of the seasonal cycles and baseline averages of individual proxies. At the end of the results section, we present hydrological model data for river discharge and sediment yield to test how well corals directly record river runoff for the three rivers influencing our corals.

3.1 Seasonal and interannual variability of Ba/Ca and G/B between cores associated with the Antainambalana watershed

For the common period of 1991 to 2005, interannual variations in Ba/Ca and G/B, for the cores MAS1 and MAS3, were compared in order to test their reproducibility (Table 2). For Ba/Ca, we measured both cores with LA-ICP-MS (LA-) and replicated MAS1 with solution ICP-MS on a monthly resolution. The mean Ba/Ca between cores and techniques differed, with MAS3 having the lowest baseline of $5.51 \pm 0.71 \mu\text{mol mol}^{-1}$. The mean Ba/Ca measured by LA- and solution ICP-MS for MAS1 were $6.05 \pm 0.75 \mu\text{mol mol}^{-1}$ and $6.75 \pm 0.78 \mu\text{mol mol}^{-1}$, respectively, with standard deviations (1σ) overlapping (Table 3). The interannual variations between cores were highly reproducible and statistically significant (> 95%), with annual mean MAS1 and MAS3 LA-ICP-MS Ba/Ca sharing 78% ($R = 0.88$; $P < 0.01$) of the variance (Fig. 3). MAS1 LA- and solution ICP-MS data shared 52% ($R = 0.72$; $P < 0.01$) of the variance.

The interannual variations in G/B profiles for MAS1 and MAS3 for the period 1991 to 2005 were also reproducible (Fig. 3; Table 2). Seasonally, the two cores shared 90% ($R = 0.97$; $P < 0.01$) of the variance, and on annual means 45% ($R = 0.67$; $P < 0.01$); all statistically significant at the 95% level. The mean G/B between MAS1 (0.95 ± 0.03) and MAS3 (0.92 ± 0.03) differed, yet their standard deviations overlapped (Table 3). Similar to Ba/Ca, MAS3 showed the lowest baseline level in G/B.

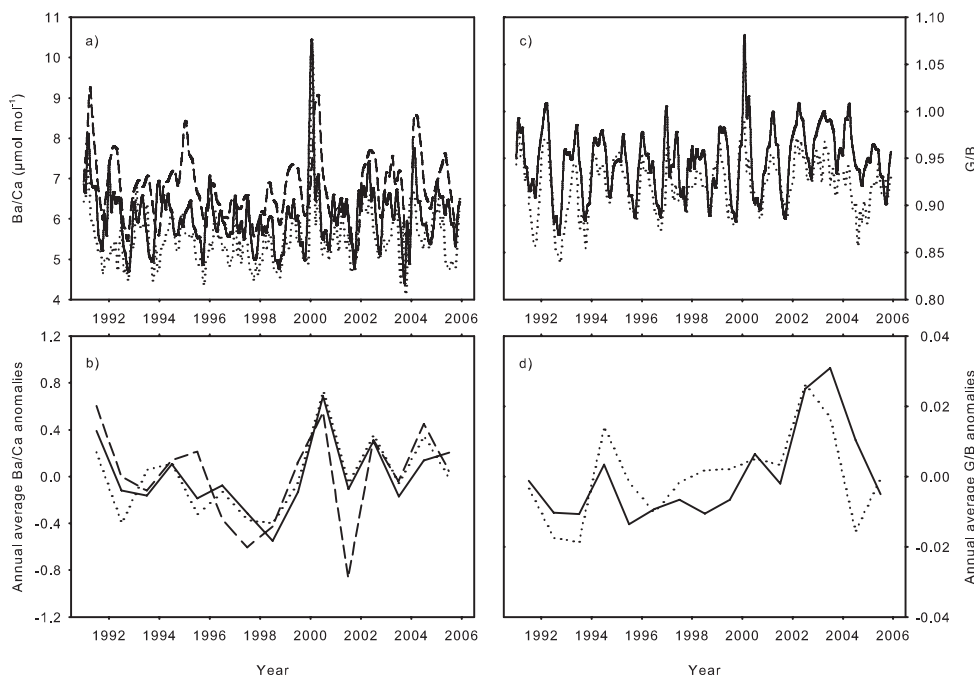


Fig. 3. The three monthly Ba/Ca (left) profiles and two G/B (right) profiles between January 1991 and December 2005, signifying proxy reproducibility in both seasonality and interannual variability. The three Ba/Ca profiles (a and b) include LA- MAS1 (solid), LA- MAS3 (dotted) and solution ICP-MS MAS1 (dashed). The two G/B profiles (c and d) include MAS1 (solid) and MAS3 (dotted). Absolute values are shown for Ba/Ca and G/B in the upper plots (a and c, respectively), and annual anomalies for both Ba/Ca and G/B are shown in the lower plots (b and d, respectively).

3.2 Seasonal and interannual variability of four river runoff proxies associated with three individual watersheds

Here, we compare G/B profiles and geochemical data for three coral cores associated with three individual watersheds across Antongil Bay. Geochemical data were measured on splits of the same powdered coral samples representing approximately 1 month of growth for individual cores. The three cores, MAS1, ANDRA and IFAHO, showed strong seasonal cycles in the monthly G/B time series for the 15 yr period studied, from January 1991 to December 2005 (Fig. 4). Similarly, strong seasonal cycles were observed in the monthly Ba/Ca time series of MAS1 and IFAHO, yet the seasonal cycles of ANDRA were not as clearly defined (Fig. 4). We followed the method of Ren et al. (2002) to calculate $\delta^{18}\text{O}_{\text{sw}}$, which assumes that coral Sr/Ca is solely a function of SST and that coral $\delta^{18}\text{O}$ is a function of both SST and $\delta^{18}\text{O}_{\text{sw}}$ (Figs. A1 and A2). The $\delta^{18}\text{O}_{\text{sw}}$ and $\delta^{13}\text{C}$ seasonal cycles of MAS1 were both strong and well defined (Figs. A3 and A4). However, in ANDRA and IFAHO the $\delta^{18}\text{O}_{\text{sw}}$ and $\delta^{13}\text{C}$ seasonal cycles were less defined yet showed strong variability (Figs. A3 and A4).

For annual averages, luminescence (G/B) showed the highest spatial correlations between the three cores/regions

for the 15 yr period out of all proxies studied ($n = 15$). ANDRA luminescence was statistically correlated with both MAS1 ($R = 0.69$; $P = 0.005$) and IFAHO ($R = 0.63$; $P = 0.013$) (Table 2). The relationship between MAS1 and IFAHO luminescence was just outside of the significance level ($R = 0.50$; $P = 0.056$). This relationship was significant, however, when considering the seasonal data (Table 2).

Conversely, the strongest and only statistically significant annual average Ba/Ca relationship was between cores MAS1 and IFAHO ($R = 0.66$; $P = 0.008$) (Table 2). ANDRA Ba/Ca showed a weaker relationship with both MAS1 ($R = 0.37$; $P = 0.17$) and IFAHO ($R = 0.27$; $P = 0.32$), which were not significant (Table 2).

The strongest relationship between average annual $\delta^{18}\text{O}_{\text{sw}}$ values was again between MAS1 and IFAHO ($R = 0.41$; $P = 0.13$), yet not significant (Table 2). This relationship was significant, however, when considering the seasonal data (Table 2). The correlation coefficients of ANDRA $\delta^{18}\text{O}_{\text{sw}}$ with MAS1 and IFAHO $\delta^{18}\text{O}_{\text{sw}}$ were lower and not significant (Table 2).

The strongest relationship between average annual $\delta^{13}\text{C}$ values was between ANDRA and IFAHO ($R = 0.32$; $P = 0.25$), yet not significant (Table 2). The correlation coefficients of MAS1 $\delta^{13}\text{C}$ with ANDRA and IFAHO $\delta^{13}\text{C}$ were both lower and also not significant (Table 2).

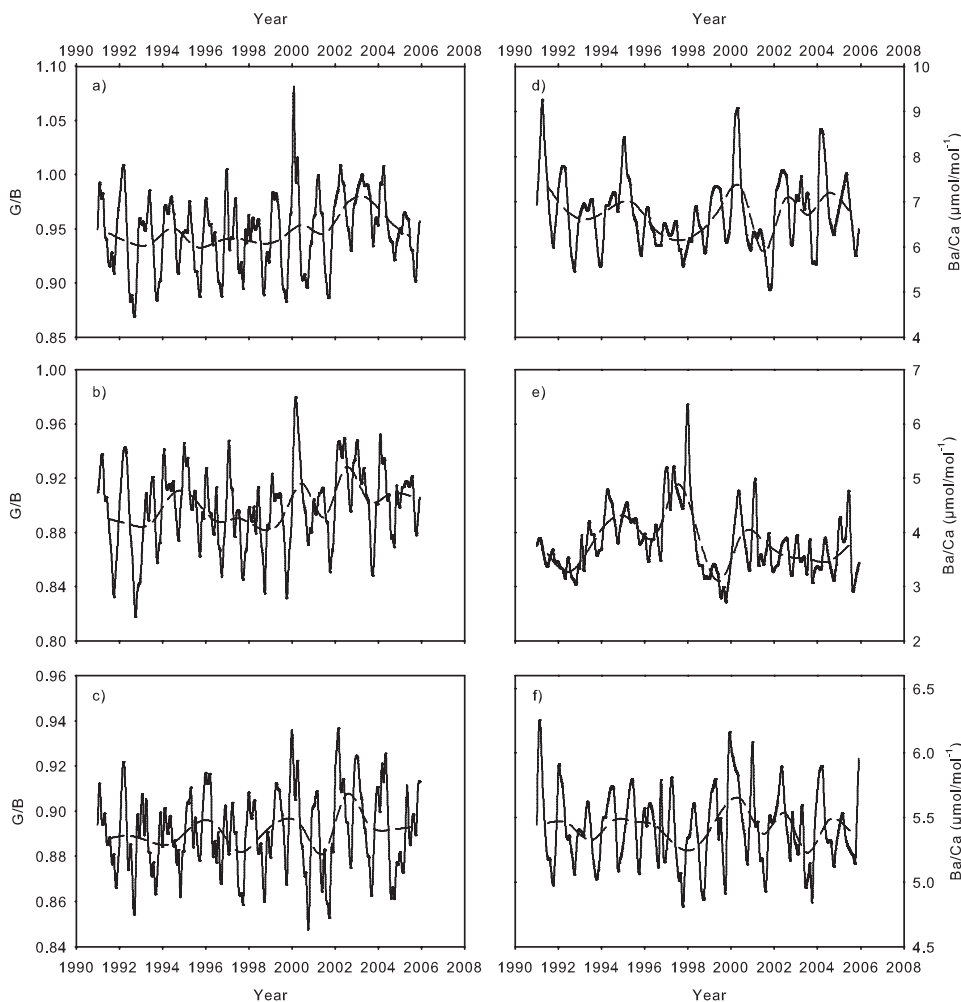


Fig. 4. Monthly G/B (a, b and c) and Ba/Ca (d, e and f) time-series over the 15 yr period between 1991 and 2005 for the three corals MAS1 (a and d), ANDRA (b and e) and IFAHO (c and f). The annual average (dashed line) G/B (a, b and c) and Ba/Ca (d, e and f) values were calculated by averaging the months January to December for each of the 15 yr.

3.2.1 Luminescence (G/B) seasonal cycles and baseline averages

Comparing the 15 yr time series of all three G/B records revealed differences in baseline values and signal amplitudes (Fig. 5a). MAS1 G/B had the highest mean value and standard deviation (0.95 ± 0.034) compared to ANDRA (0.90 ± 0.029) and IFAHO (0.89 ± 0.018) (Table 3). Moreover, ANDRA and IFAHO had similar mean values. However, the signal amplitude of ANDRA was far greater than IFAHO (Fig. 5a). During the dry season ANDRA G/B was below IFAHO G/B, yet during the wet season ANDRA G/B was higher. This is further highlighted by the mean seasonal cycles of G/B for the three cores (Fig. 6). Here, it becomes clear that the MAS1 G/B signal was far higher than both the ANDRA and IFAHO G/B signals for the entire calendar year, while the ANDRA G/B signal overtakes the IFAHO

G/B signal during the wet season. Standard deviations indicate the variability of each site over the 15 yr period (Fig. 6), with MAS1 G/B overlapping ANDRA (not IFAHO) only in four out of twelve calendar months. Three of those four months were in the dry season.

3.2.2 Ba/Ca seasonal cycles and baseline averages

The most noticeable contrast between the G/B and Ba/Ca time series was in their respective baseline averages (Fig. 5b). Although the MAS1 Ba/Ca mean value ($6.75 \pm 0.78 \mu\text{mol mol}^{-1}$) was highest of the three records, similar to the results of G/B, a significant difference between the mean Ba/Ca values of ANDRA and IFAHO was observed (Fig. 5b and Table 3). The mean IFAHO Ba/Ca value ($5.42 \pm 0.28 \mu\text{mol mol}^{-1}$) was significantly higher than ANDRA ($3.80 \pm 0.58 \mu\text{mol mol}^{-1}$), despite the higher range and variability of ANDRA (Table 3). This contrast in results

Table 3. Statistical description of coral proxy data for MAS1 (upper), MAS3 (middle upper), ANDRA (middle lower) and IFAHO (lower). The mean, standard deviation (SD), range, maximum value (Max) and minimum value (Min) were calculated from the monthly interpolated data spanning January 1991 till December 2005 (15 yr). The proxy data include G/B, Ba/Ca (two methods), $\delta^{18}\text{O}_{\text{sw}}$, $\delta^{13}\text{C}$ and reconstructed salinity based on the $\delta^{18}\text{O}_{\text{sw}}$ (Fig. 7).

	Mean	SD	Range	Max	Min
MAS1					
G/B	0.95	0.03	0.21	1.08	0.87
Ba/Ca ($\mu\text{mol mol}^{-1}$) – HR-ICP-MS	6.75	0.78	4.20	9.26	5.06
Ba/Ca ($\mu\text{mol mol}^{-1}$) – LA-ICP-MS	6.05	0.75	5.56	10.06	4.50
$\delta^{18}\text{O}_{\text{sw}}$ (‰)	−0.50	0.40	1.79	0.26	−1.53
Reconstructed salinity (psu)	25.54	2.93	13.25	31.17	17.92
$\delta^{13}\text{C}$ (‰)	−3.01	0.58	2.83	−1.89	−4.72
MAS3					
G/B	0.92	0.03	0.15	0.98	0.84
Ba/Ca ($\mu\text{mol mol}^{-1}$) – LA-ICP-MS	5.51	0.71	5.69	9.88	4.19
ANDRA					
G/B	0.90	0.03	0.16	0.98	0.82
Ba/Ca ($\mu\text{mol mol}^{-1}$) – HR-ICP-MS	3.80	0.58	3.61	6.38	2.71
$\delta^{18}\text{O}_{\text{sw}}$ (‰)	0.17	0.28	1.53	0.82	−0.72
Reconstructed salinity (psu)	30.55	2.07	11.37	35.33	23.96
$\delta^{13}\text{C}$ (‰)	−3.33	0.65	2.76	−2.01	−4.77
IFAHO					
G/B	0.89	0.018	0.09	0.94	0.85
Ba/Ca ($\mu\text{mol mol}^{-1}$) – HR-ICP-MS	5.42	0.28	1.39	6.21	4.81
$\delta^{18}\text{O}_{\text{sw}}$ (‰)	−0.27	0.20	1.07	0.21	−0.86
Reconstructed salinity (psu)	27.26	1.50	7.91	30.80	22.89
$\delta^{13}\text{C}$ (‰)	−2.83	0.45	2.79	−2.09	−4.88

is further emphasised when comparing the mean seasonal cycles of the three Ba/Ca records (Fig. 6). Only in November and December was there an overlap in standard deviations between MAS1 and IFAHO (Fig. 6). All ANDRA monthly Ba/Ca values were significantly below the Ba/Ca values of IFAHO. Further, a small decrease was observed in the Ba/Ca signal of ANDRA occurring between February and May (wet season). This was not the case for MAS1 or IFAHO (Fig. 6).

3.2.3 $\delta^{18}\text{O}_{\text{sw}}$ seasonal cycles and baseline averages

Measuring the salinity and $\delta^{18}\text{O}$ of seawater samples, we established a regional regression equation and applied it to transform coral derived $\delta^{18}\text{O}_{\text{sw}}$ values into reconstructed salinities (Fig. 7). The core with the most negative mean $\delta^{18}\text{O}_{\text{sw}}$ value (-0.50 ± 0.39 ‰) was MAS1 (Table 2). When converting the skeletal $\delta^{18}\text{O}_{\text{sw}}$ signal, the mean reconstructed salinity of MAS1 equated to 25.54 ± 2.93 psu (Table 3). IFAHO had a mean $\delta^{18}\text{O}_{\text{sw}}$ value of -0.27 ± 0.20 ‰, which equated to a mean reconstructed salinity of 27.26 ± 1.50 psu (Table 3). The most positive mean $\delta^{18}\text{O}_{\text{sw}}$ value was ANDRA (0.17 ± 0.28 ‰), equating to the highest mean recon-

structed salinity of 30.55 ± 2.07 psu (Table 3). The standard deviations given for the mean $\delta^{18}\text{O}_{\text{sw}}$ seasonal cycles of MAS1 and IFAHO overlap in every month with the exception of February (Fig. 6). Both showed a mean seasonal $\delta^{18}\text{O}_{\text{sw}}$ cycle decreasing during the wet season and increasing during the dry season (albeit IFAHO values start to increase earlier than MAS1) (Fig. 6). This is not the case for ANDRA, which showed a reverse mean seasonal cycle whereby $\delta^{18}\text{O}_{\text{sw}}$ values increased during the wet season and decreased during the dry season (Fig. 6). Moreover, during the months November to February there was no overlap of standard deviations between IFAHO and ANDRA as the $\delta^{18}\text{O}_{\text{sw}}$ values of IFAHO were significantly more negative than ANDRA (Fig. 6).

3.2.4 $\delta^{13}\text{C}$ seasonal cycles and baseline averages

Core ANDRA gave the most negative mean $\delta^{13}\text{C}$ signal, being -3.33 ± 0.65 ‰ (Table 3). The core with the most positive mean $\delta^{13}\text{C}$ signal was IFAHO (-2.83 ± 0.45 ‰), whereas MAS1 measured -3.01 ± 0.58 ‰ (Table 3). All cores showed high variability over the 15 yr period (Table 3). Moreover, the monthly standard deviations given for

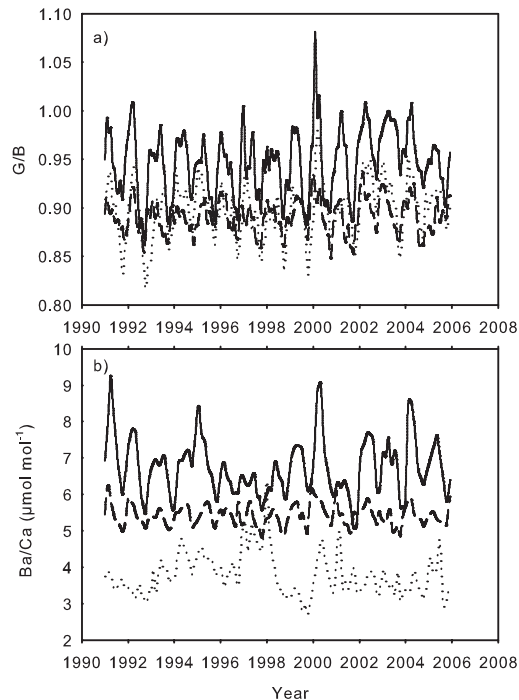


Fig. 5. Cross-core comparison of monthly G/B (a) and Ba/Ca (b) absolute values for the complete 15 yr time-series of the three cores MAS1 (solid), ANDRA (dotted) and IFAHO (dashed).

the $\delta^{13}\text{C}$ mean seasonal cycles indicate that individual $\delta^{13}\text{C}$ baseline values were statistically similar over the 15 yr (Fig. 6 and Table 3). Further, the mean seasonal cycles were inconsistent between cores as both IFAHO and MAS1 showed a depleted $\delta^{13}\text{C}$ signal during the wet season and an enrichment during the dry season (albeit IFAHO again enriched earlier than MAS1), whereas, ANDRA showed a bimodal cycle (Fig. 6).

3.3 Hydrological model data

3.3.1 River discharge

The river with the highest modelled discharge was the Antainambalana, associated with coral MAS1, which had a mean discharge rate of $260 \pm 92 \text{ m}^3 \text{ s}^{-1}$ (Table 4). The rivers Ambanizana and Anaovandran, associated with corals ANDRA and IFAHO, respectively, had a statistically similar modelled discharge rate, however, of significantly lower magnitude to the river Antainambalana (Table 4). The mean discharge rate of the Anaovandran ($8.2 \pm 4.7 \text{ m}^3 \text{ s}^{-1}$) was slightly higher than the Ambanizana ($6.8 \pm 4.0 \text{ m}^3 \text{ s}^{-1}$). This order of relative discharge rate between the three rivers was similar to the proxy results of G/B (Fig. 6).

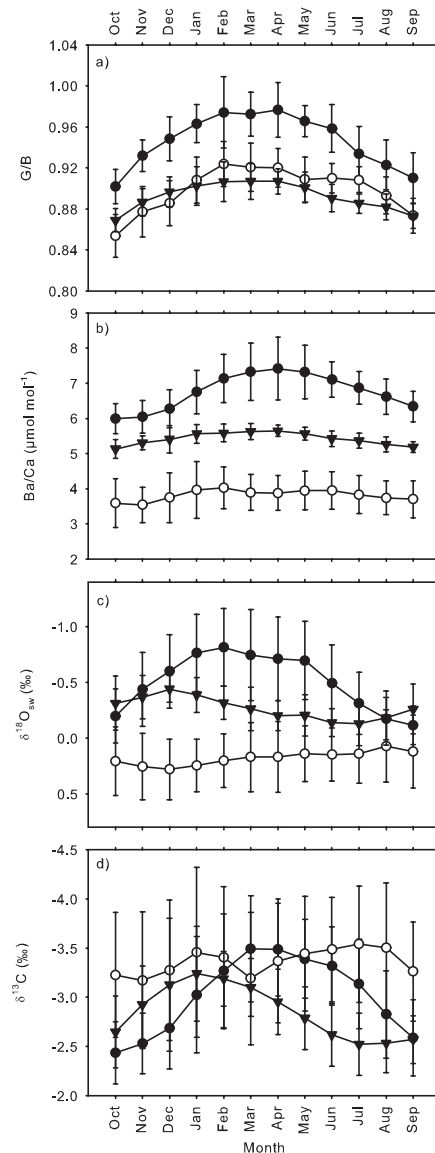


Fig. 6. Monthly averaged G/B (a), Ba/Ca (b), $\delta^{18}\text{O}_{\text{sw}}$ (c) and $\delta^{13}\text{C}$ (d) for MAS1 (solid circles), ANDRA (open circles) and IFAHO (triangles), indicating the average seasonal cycles. Monthly averages were calculated for the 15 yr period spanning January 1991 till December 2005. The standard deviations for individual months are given as error bars. The $\delta^{18}\text{O}_{\text{sw}}$ and $\delta^{13}\text{C}$ is given relative to V-PDB.

3.3.2 Sediment runoff

The river with the highest modelled sediment runoff was the Antainambalana, associated with coral MAS1, which also recorded the highest Ba/Ca values (Fig. 6b and Table 4). However, unlike the modelled discharge data, there was a significant difference between the modelled sediment runoff of the two other rivers (Table 4). The modelled sediment runoff for the river Ambanizana, associated with coral ANDRA was

Table 4. Statistical description of modelled river discharge (upper) and sediment yield (lower) data for the three river catchments Antainambalana, Ambanizana and Anaovandran; the closest rivers to corals MAS1, ANDRA and IFAHO, respectively. The mean, standard deviation (SD), range, maximum value (Max) and minimum value (Min) are calculated from the mean annual data spanning 15 yr (1991–2005).

River discharge ($\text{m}^3 \text{s}^{-1}$)	Mean	SD	Range	Max	Min
Antainambalana	260	92	440	530	93
Ambanizana	6.8	4.0	19	19	0.88
Anaovandran	8.2	4.7	22	23	1.6
Sediment runoff (kg yr^{-1})	Mean	SD	Range	Max	Min
Antainambalana	1.10×10^9	0.39×10^9	1.36×10^9	2.03×10^9	6.78×10^8
Ambanizana	1.72×10^8	9.73×10^7	3.35×10^8	3.88×10^8	5.35×10^7
Anaovandran	9.31×10^6	4.57×10^6	1.76×10^7	2.24×10^7	4.83×10^6

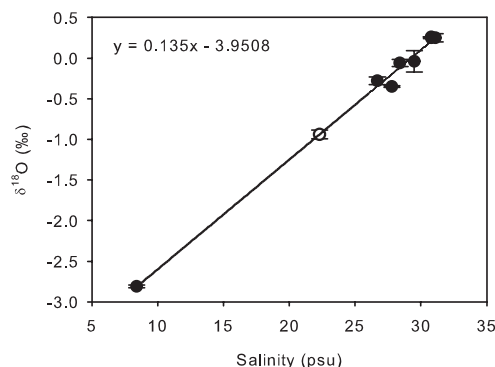


Fig. 7. Calibration of the $\delta^{18}\text{O}$ of water samples with salinity measurements used to reconstruct salinity from coral $\delta^{18}\text{O}_{\text{sw}}$. All data points are given as averages of two samples taken during the dry season (solid circles) and wet season (open circle). The standard deviation is given as error bars.

significantly higher than for the river Anaovandran, associated with the coral IFAHO (Table 4). The relative order of sediment runoff rates between the rivers ANDRA and IFAHO is opposite to those of the Ba/Ca results, as ANDRA Ba/Ca values were lowest (Fig. 6b).

4 Discussion

4.1 Reproducibility of Ba/Ca and G/B between cores (MAS1 and MAS3) from the same watershed

We demonstrate that two coral cores from the same watershed in Antongil Bay share a significant amount of interannual variation in both Ba/Ca and G/B (Fig. 3). This indicates that both of these terrestrial runoff proxies respond to a common environmental signal. These results are in agreement with previous analyses, in which G/B signals were

compared on longer time scales between the coral cores MAS1 and MAS3 (Grove et al., 2010). Grove et al. (2010) used 100 yr of G/B data, which revealed an even higher correlation than for the 15 yr period considered here. A comparison of Ba/Ca and G/B was only performed for core MAS1, which showed a significant correlation for annual mean values (Grove et al., 2010).

Here, we replicated Ba/Ca for a second core (MAS3) and can confirm that interannual variations for this particular watershed are reproducible (Fig. 3). This agrees with similar studies from adjacent watersheds in the Great Barrier Reef (GBR), where Ba/Ca profiles showed significant correlations between cores (Alibert et al., 2003). Slight offsets in mean Ba/Ca and G/B signals between MAS1 and MAS3 are most likely related to different hydrodynamic regimes of flood plume currents between the reef slope (MAS1) and reef flat (MAS3) sites along the Nosy Mangabe island fringing reef. Similar small-scale differences in terrestrial runoff proxies have been observed for GBR catchments related to ‘island wake’ effects (Jupiter et al., 2008; Lewis et al., 2011).

The differences in absolute values observed between LA-Ba/Ca and solution ICP-MS Ba/Ca in MAS1 are likely related to time averaging in monthly milled samples compared to sub-weekly LA- data (Fig. 3). However, the relative changes in Ba/Ca do share 52 % of the variability between different techniques and the main sediment runoff spikes were reproducible, i.e. years 1991, 2000.

4.2 Spatial linkages between coral proxies of terrestrial runoff across Antongil Bay

Proxy validation is a common problem in coral palaeoclimatology, as long-term in-situ data are rarely available (Jones et al., 2009). Lower resolution data are often applied as a substitute to calibrate proxies, i.e. satellite and model data (Corrège, 2006; Reynolds et al., 2002; Quartly et al., 2007). In this study, luminescence was the only proxy to show a considerable relationship between all three corals. For the

majority of other proxies, vital effects and localised differences were likely more dominant than the regional climate signal expressed in the values. To best understand these differences between river signals at individual corals and at their respective river mouths, we compared our proxy data with hydrological model data. Although not ideal, the model data give a good indication of both sediment yield and river discharge for the three watersheds studied.

A strong relationship was observed between annual average G/B of the three coral cores MAS1, ANDRA and IFAHO, suggesting that corals are recording a regional signal likely reflecting HA runoff. This argument is further strengthened when considering the modelled discharge data. Core MAS1 and the river Antainambalana (associated with MAS1) showed highest G/B values and modelled discharge, respectively, compared to the other two cores/ivers. Moreover, corals ANDRA and IFAHO showed statistically similar baseline averages in G/B, again replicated by the modelled discharge data. As HA runoff is linked to river discharge (Lough, 2011a; Grove et al., 2010), this likely explains the patterns observed in our corals. The only contrast between the two datasets was that ANDRA G/B peaked above IFAHO G/B during the wet season. Discharge data suggest otherwise, whereby the mean, range, maximum and minimum river discharge of Ambanizana, associated with coral ANDRA, are all less than the Anaovandran, associated with the coral IFAHO. At this stage, we cannot exclude the possibility that the recorded discharge signal at coral ANDRA may also be influenced by adjacent rivers. Also, in contrast to the large watershed of the Antainambalana, the rivers influencing ANDRA and IFAHO have much smaller watersheds, which increases uncertainties in modelled discharge due to the relatively large model grid size (50 km).

When considering both the $\delta^{18}\text{O}_{\text{sw}}$ baseline averages and mean seasonal cycles, it becomes clear that strong hydrographic differences exist between the three coral sites. Coral MAS1 recorded the freshest waters, comparable to the modelled discharge rates for the Antainambalana. However, the reconstructed salinity signal at ANDRA indicated most saline conditions as well as a slightly reversed mean seasonal water cycle (Fig. 6c). As both the river Ambanizana and Anaovandran, associated with ANDRA and IFAHO respectively, have similar watershed sizes and modelled discharge rates, the $\delta^{18}\text{O}_{\text{sw}}$ baseline averages and seasonal cycles were expected to be similar. Such inconsistencies are likely a result of a difference between the distances from the river mouth to the coral.

Coral ANDRA is located 7 km from the Ambanizana river mouth, compared to IFAHO, which lies 4.5 km from the Anaovandran. The river signal at ANDRA is therefore likely to have been diluted by seawater via conservative mixing more than the signal at IFAHO, giving it a higher recorded salinity. Alternatively, the higher salinity signal at ANDRA may be linked to currents. As coral ANDRA is located further from the river mouth than IFAHO, it is increasingly

likely that currents may channel the freshwater signal, associated with the river Ambanizana, away from the coral head. Nevertheless, according to proxy data, coral ANDRA receives no freshwater signal during the warm/wet season, and furthermore, has a slight increase in salinity. This increase might be related to the $\delta^{18}\text{O}$ hydrological balance (evaporation) of the water body influencing ANDRA at this time.

Comparing the Ba/Ca signals between cores and with modelled runoff data augments the argument that coral ANDRA is not influenced by runoff from the river Ambanizana. Coral MAS1 showed the highest recorded levels of Ba/Ca compared to the other two corals, which is in agreement with the modelled data, as the river Antainambalana had the highest modelled sediment runoff. As the Ba/Ca annual averages of MAS1 and IFAHO are statistically correlated, they seem to be recording a regional sediment runoff signal (Sinclair and McCulloch, 2004; Alibert et al., 2003; McCulloch et al., 2003; Fleitmann et al., 2007). Coral IFAHO showed a significantly lower mean Ba/Ca signal. This signifies that the source input at the river Anaovandran is considerably lower than the river Antainambalana, which is again in agreement with modelled sediment runoff data.

Model data for the river Ambanizana, associated with coral ANDRA, indicates that sediment runoff is far higher than that of the river Anaovandran, associated with IFAHO. ANDRA resides a further 2.5 km from its river source than IFAHO, therefore any river signal from the Ambanizana would be diluted/mixed by seawater for an extra 2.5 km. However, given the significantly higher modelled sediment runoff for the Ambanizana, it is expected that ANDRA Ba/Ca would still be higher or similar to IFAHO. This is not the case, as the Ba/Ca signal in ANDRA is significantly less than IFAHO. Given that the annual average Ba/Ca results of ANDRA do not correlate with either MAS1 or IFAHO, it is therefore likely that (1) skeletal Ba/Ca variability is linked to a different source other than sediment runoff, (2) skeletal Ba/Ca variability is derived from the largest watershed and its Ba/Ca signature is well mixed and diminished before arriving at the coral site, and/or (3) low sediment runoff is associated with the river Ambanizana watershed, contrary to what modelled data suggest.

Although ANDRA and IFAHO catchments have similar sizes and draw from the same mountains covered in dense rainforest, differences in hinterland topography and vegetation cover prevail. Such differences should also be considered when explaining the patterns observed between Ba and HA. The ANDRA river watershed follows a valley with a steep slope covered with rainforest (Figs. 1 and 3 in Kremen et al., 1999). The river associated with IFAHO drains from a shallower slope and eventually runs through a plain with less vegetation cover (Windley et al., 1994 and references therein; Figs. 1 and 3 in Kremen et al., 1999). This shallow slope allowed for easy human settlement and subsequent deforestation (Figs. 1 and 3 in Kremen et al., 1999; Green and Sussman, 1990). The difference in slope influences the flow

speed and thus the amount and type of dissolved and particulate transports (Milliman and Syvtski, 1992; Larsen and Webb, 2009). The continuous vegetation cover at ANDRA binds and protects sediment from erosion but allows leaching of HA, while the plain at IFAHO is much less densely vegetated, most likely facilitating sediment erosion (Douglas, 1967). HA input from the river source associated with ANDRA would therefore be higher than that of IFAHO, as more dissolved HA are leached from a watershed with a denser vegetation cover, thus flushing more dissolved HA down the steep gradients into the marine system. As the vegetation retains sediments, this might also partly explain why Ba levels at ANDRA are low. However, modelled sediment yield suggest otherwise, which indeed takes factors such as elevation, slope, soils, etc. into account.

Previous studies have also found no relationship between Ba/Ca and river discharge across a water quality gradient (Jupiter et al., 2008; Prouty et al., 2010; Lewis et al., 2011). Again, in contrast to the large watershed of the Antainambalana, the rivers influencing ANDRA and IFAHO have much smaller watersheds, which increases uncertainties in modelled sediment yield due to the large model grid size. Furthermore, the model data indicate the sediment yield at the river mouth whereas the corals record the ambient Ba/Ca signals (not sediment) at the reef site along a water quality gradient (Lewis et al., 2011).

The low Ba/Ca values and high reconstructed salinities of ANDRA provide evidence that the river Ambanizana is only marginally influencing the coral site. Yet, the high G/B values suggest otherwise, indicating that a runoff signal does exist during the wet season. Indeed, the strongest annual average G/B relationship observed between cores was between coral MAS1 and ANDRA. Therefore, it is more likely that the HA signal reaching coral ANDRA is a mixture of signals originating from the river Antainambalana, associated with MAS1, and the river Ambanizana, associated with ANDRA. This is plausible given the clockwise direction of the currents within the bay (Fig. 1), the high concentrations of HA associated with each watershed and the conservative mixing nature of HA (Bowers and Brett, 2008). Unlike HA, barium behaves non-conservatively in estuaries, as it is influenced by processes such as phytoplankton cycling (Sinclair, 2005; Hanor and Chan, 1977; Coffey et al., 1997). Therefore, the riverine Ba signal associated with MAS1 may well have diminished by the time it reached coral ANDRA. Further, the salinity signal ($\delta^{18}\text{O}_{\text{sw}}$) from the Antainambalana may have been lost due to mixing of different water masses (Fig. 7). As HA are conservative and are only associated with terrestrial inputs, they are duly transported to and recorded by coral ANDRA.

The skeletal $\delta^{13}\text{C}$ signals of all three cores showed similar baseline averages and high standard deviations, making it difficult to statistically differentiate between signals. Coral $\delta^{13}\text{C}$ can be affected by a number of vital effects including kinetic effects, light, pH variation at sites of calcifica-

tion, skeletal architecture and the influence of metabolic CO_2 (McConnaughey, 2003; Felis et al., 2003; Rollion-Bard et al., 2003), which have likely influenced the $\delta^{13}\text{C}$ variability within and between cores. Nevertheless, the mean seasonal cycles of MAS1 and IFAHO showed a depletion during the wet season. This probably reflects either a depleted $\delta^{13}\text{C}$ signal of DIC associated with the river plume (Moyer, 2008; von Fischer and Tieszen, 1995; Swart et al., 1996; Marin-Spiotta et al., 2008; Moyer and Grottoli, 2011), or a decrease in photosynthesis reducing the depletion of ^{12}C in the carbon pool (Grottoli, 2002; Grottoli and Wellington, 1999; Weil et al., 1981; Swart et al., 1996; Reynaud-Vaganay et al., 2001; Reynaud et al., 2002). Both would yield an inverse relationship with increasing runoff. As the freshest waters are associated with coral MAS1, this might explain the more depleted $\delta^{13}\text{C}$ values compared to IFAHO.

The $\delta^{13}\text{C}$ signal of coral ANDRA was more depleted than both MAS1 and IFAHO. This is surprising as it was not influenced by discharge directly, and therefore values were expected to be more enriched (Moyer, 2008; von Fischer and Tieszen, 1995; Swart et al., 1996; Marin-Spiotta et al., 2008; Moyer and Grottoli, 2011). Further, the mean seasonal cycle of ANDRA $\delta^{13}\text{C}$ was bimodal, as both $\delta^{13}\text{C}$ enrichment occurred during the peak runoff season as well as the dry season. As ANDRA is not (or only marginally) influenced by runoff, there are likely many other factors contributing to skeletal $\delta^{13}\text{C}$ variability and the baseline average, including ambient seawater productivity. Interestingly, the mean seasonal cycle of Ba/Ca in ANDRA also showed a decrease in March when $\delta^{13}\text{C}$ enriched slightly (Fig. 6). This may be linked to phytoplankton uptake of Ba during peak runoff, when nutrients are plentiful, causing enrichment of $\delta^{13}\text{C}$ due to the preferential uptake of ^{12}C by phytoplankton (Sinclair, 2005 and references therein; Stecher and Kogut, 1999). An increase in primary production causes Ba to be scavenged from the water column due to the active cycling of algal blooms (Sinclair, 2005; Stecher and Kogut, 1999). As the nutrient levels are reduced, decaying algae will increase Ba concentrations within the water column by recycling. Correlating the annual average Ba/Ca values with the annual average $\delta^{13}\text{C}$ values indeed gives an indication that this is the case. Although not statistically significant, ANDRA gave the highest correlation ($R = 0.46$; $P = 0.086$), compared to MAS1 ($R = 0.029$) and IFAHO ($R = 0.13$).

In this study we demonstrate that Ba/Ca and G/B signals from the same watershed are reproducible. However, strong localised signals are observed between cores associated with different watersheds due to the large distances separating the corals. G/B was the only proxy which showed a regional similarity across the bay, although the relationship between MAS1 and IFAHO was just outside the 5% significance level. A strong relationship was observed in Ba/Ca for MAS1 and IFAHO, yet not with ANDRA. This is likely related to ANDRA residing a further 2.5 km from its associated river mouth compared to IFAHO and topographic

and vegetation cover differences between watersheds, despite having a similar sizes. No significant regional signal was observed for $\delta^{18}\text{O}_{\text{sw}}$ and $\delta^{13}\text{C}$. The $\delta^{13}\text{C}$ signal was likely overwhelmed by coral vital effects and in-situ productivity, whereas the $\delta^{18}\text{O}_{\text{sw}}$ signals are likely inconsistent due to a combination of vital effects and site-specific environmental differences in the hydrological balance.

Discrepancies between the proxy results and modelled data indicate that corals are not ideally suited for directly comparing river systems. Absolute proxy values give an indication of the ambient concentration surrounding the coral at the time of precipitation, yet not the source input. Prouty et al. (2010) compare Ba/Ca baselines for Hawaiian corals to other published Ba/Ca records from the GBR (McCulloch et al., 2003) and Kenya (Fleitmann et al., 2007), relating differences to river input. This is problematic since the Ba/Ca signal at each site reflects both the distance from the source and the source input. Moreover, mixing gradients (distance), currents, proxy behaviour and vital effects can all influence the precipitated skeletal signal significantly from the moment it leaves the river source. In a recent study, Lewis et al. (2011) provided evidence of the impact small-scale hydrodynamic differences have on skeletal Ba/Ca across the complex hydrography of reefs in the GBR from multiple cores across a water quality gradient. However, by combining runoff proxies and comparing baseline averages and mean seasonal cycles, aided by hydrological model data, a good overview of the runoff products influencing the coral sites was achieved in our study. Moreover, all proxies provide information on the runoff dynamics of the bay system, which will assist both terrestrial and marine management programmes in Madagascar.

5 Conclusions

Models provide an estimate of discharge and sediment runoff at the mouth of a river, whereas corals record a signal potentially several kilometres away. Subsequently, the riverine signal can be modified by the time it reaches the coral. The distance from the river source is a primary reason why comparing absolute runoff proxy values to differentiate between watersheds is unreliable. The further a coral resides from the river mouth, the more the proxy signal is mixed/diluted by seawater. Depending on the behaviour of the proxy, the distance from the river can also have dramatic effects on the recorded signal at the coral. Proxies such as Ba/Ca and $\delta^{13}\text{C}$ are non-conservative mixers, and therefore altered by recycling processes such as phytoplankton uptake. Nevertheless, we find Ba/Ca to be reproducible within the same watershed and also across distant watersheds given there is a close proximity of the coral to a river mouth and/or associated with a large river. Humic acids and the $\delta^{18}\text{O}$ signal mix conservatively in the water column. Indeed, there was a good regional relationship observed between coral G/B signals, making it

an ideal proxy for paleoclimate reconstructions and spatial comparisons of corals (not rivers). Yet, the skeletal $\delta^{18}\text{O}_{\text{sw}}$ signal showed little consensus between cores, which was likely due to vital effects, local differences in the hydrological balance and their vicinity to the river mouths. Other physiochemical parameters such as currents also need to be considered when interpreting proxy results. Even though a coral may reside closer to one river than another, currents can determine which river signal the coral receives. Nevertheless, comparing proxy baseline averages and mean seasonal cycles provides a good overview of the runoff dynamics over a bay system.

Appendix A

Time-series of Sr/Ca and stable isotope data

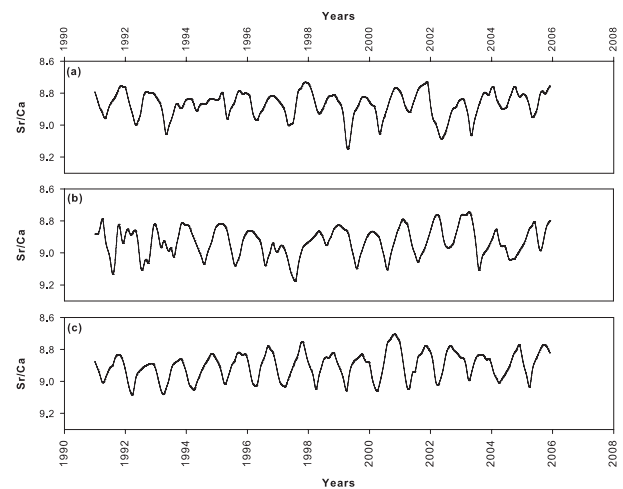


Fig. A1. The Sr/Ca time-series of coral cores MAS1 (a), ANDRA (b) and IFAHO (c) for the common period 1991–2005.

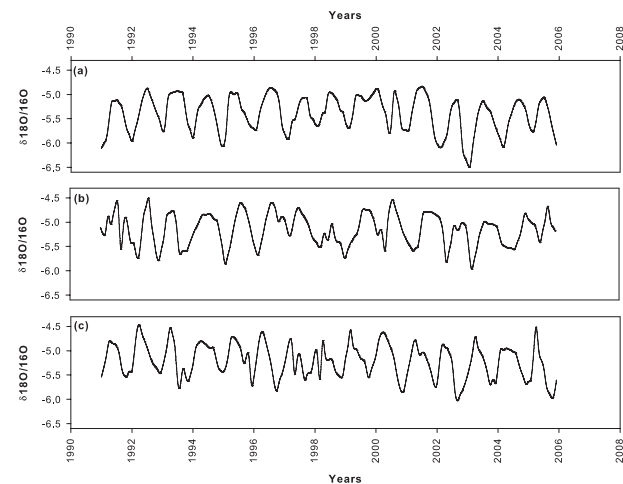


Fig. A2. The skeletal $\delta^{18}\text{O}$ time-series of coral cores MAS1 (a), ANDRA (b) and IFAHO (c) for the common period 1991–2005.

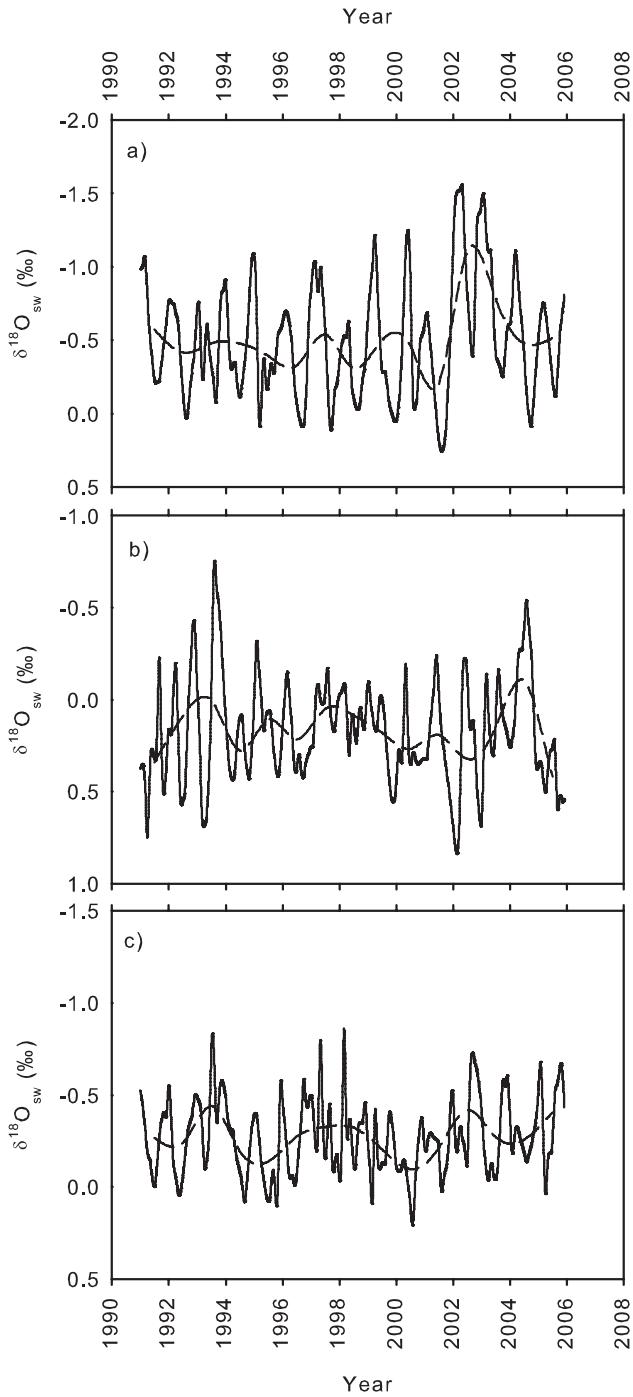


Fig. A3. The $\delta^{18}\text{O}_{\text{seawater}}$ ($\delta^{18}\text{O}_{\text{sw}}$) of coral cores MAS1 (a), AN-DRA (b) and IFAHO (c) calculated by subtracting the thermal component from coral skeletal $\delta^{18}\text{O}$ based on the relative changes in Sr/Ca-SST following Ren et al. (2002). The annual average (dashed line) values were calculated by averaging the months January to December for each of the 15 yr.

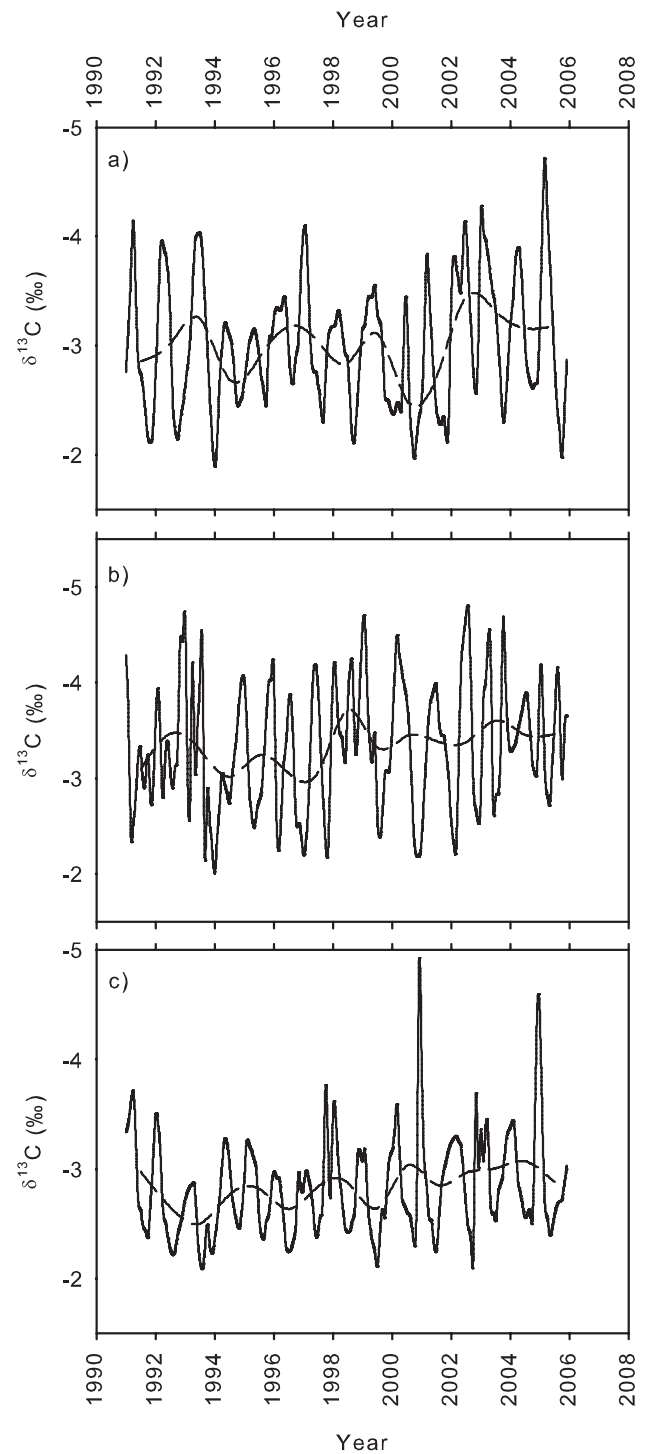


Fig. A4. The $\delta^{13}\text{C}$ of coral cores MAS1 (a), AN-DRA (b) and IFAHO (c) relative to V-PDB. The annual average (dashed line) values were calculated by averaging the months January to December for each of the 15 yr.

Acknowledgements. This work was supported as part of the SINDOCOM grant under the Dutch NWO program “Climate Variability”, grant 854.00034/035. Additional support comes from the NWO ALW project CLIMATCH, grant 820.01.009, and the Western Indian Ocean Marine Science Association through the Marine Science for Management programme under grant MASMA/CC/2010/02. We thank the Wildlife Conservation Society (WCS) Madagascar, especially Heriliala Randriamahazo and the WCS/ANGAP team in Maroantsetra, for their support in fieldwork logistics and in the organisation of the research permits, CAF/CORE Madagascar for granting the CITES permit and ANGAP Madagascar for support of our research activities in the vicinity of the marine and forest nature parks. Furthermore, we would like to thank Bob Koster and Rineke Gieles for continuous development and maintenance of the UV-Core Scanner, and Michiel Kienhuis, Suzanne Verdegaal and Evaline van Weerlee for assisting with stable isotope measurements. We thank Jan Vermaat and Hans de Moel (both VU University Amsterdam) for providing the STREAM model data outputs for Antongil Bay (Madagascar) and for discussions of the sediment yield N-SPECT model results.

Edited by: A. Shemesh

References

- Aerts, J. C. J. H. and Bouwer, L. M.: Calibration and validation for the wider Perfume River Basin in Vietnam. Commissioned report and guided by R. Misdorp RIKZ/ Coastal Zone Management Centre, The Hague, 35 pp., 2002.
- Aerts, J. C. J. H., Kriek, M., and Schepel, M.: STREAM, spatial tools for river basins and environment and analysis of management options: Set up and requirements, *Phys. Chem. Earth Pt. B*, 24, 591–595, 1999.
- Agarwal, D. K., Silander, J. A., Gelfand, A. E., Dewar, R. E., and Mickelson, J. G.: Tropical deforestation in Madagascar: analysis using hierarchical spatially explicit, Bayesian regression models, *Ecol. Model.*, 185, 105–131, 2005.
- Alibert, C. and McCulloch, M. T.: Strontium/calcium ratios in modern *Porites* corals from the Great Barrier Reef as a proxy for sea surface temperature: calibration of the thermometer and monitoring of ENSO, *Paleoceanography*, 12, 345–363, 1997.
- Alibert, C., Kinsley, L., Fallon, S. J., McCulloch, M. T., Berkelmans, R., and McAllister, F.: Source of trace element variability in Great Barrier Reef corals affected by the Burdekin flood plumes, *Geochim. Cosmochim. Ac.*, 67, 231–246, 2003.
- Barnes, D. J. and Taylor, R. B.: On the nature and causes of luminescent lines and bands in coral skeletons, *Coral Reefs*, 19, 221–30, 2001.
- Barnes, D. J. and Taylor, R. B.: On the nature and causes of luminescent lines and bands in coral skeletons: II, Contribution of skeletal crystals, *J. Exp. Mar. Biol. Eco.*, 322, 135–142, 2005.
- Birkinshaw, C. and Randrianjanahary, M.: The effects of Cyclone Hudah on the forest of Masoala Peninsula, Madagascar, *Madagascar Conservation & Development*, 2, 17–20, 2007.
- Bowers, D. G. and Brett, H. L.: The relationship between CDOM and salinity in estuaries: An analytical and graphical solution, *J. Marine. Syst.*, 73, 1–7, 2008.
- Bouwer, L. M., Aerts, J. C. J. H., Droogers, P., and Dolman, A. J.: Detecting the long-term impacts from climate variability and increasing water consumption on runoff in the Krishna river basin (India), *Hydrol. Earth Syst. Sci.*, 10, 703–713, doi:10.5194/hess-10-703-2006, 2006.
- Carricart-Ganivet, J. P., Lough, J. M., and Barnes, D. J.: Growth and luminescence characteristics in skeletons of massive *Porites* from a depth gradient in the central Great Barrier Reef, *J. Exp. Mar. Biol. Ecol.*, 351, 27–36, 2007.
- Coffey, M., Dehairs, F., Collette, O., Luther, G., Church, T., and Jickells, T.: The behaviour of dissolved barium in estuaries, *Estuar. Coast. Shelf. S.*, 45, 113–121, 1997.
- Cole, J. E., Dunbar, R. B., McClanahan, T. R., and Muthiga, N. A.: Tropical Pacific forcing of decadal SST variability in the Western Indian Ocean over the past two centuries, *Science*, 287, 617–619, 2000.
- Collins, A. S.: Madagascar and the amalgamation of Central Gondwana, *Gondwana Res.*, 9, 3–16, 2006.
- Corrège, T.: Sea surface temperature and salinity reconstructions from coral geochemical tracers, *Palaeogeogr. Palaeoclimatol.*, 232, 408–428, 2006.
- DeLong, K. L., Quinn, T. M., and Taylor, F. W.: Reconstructing twentieth-century sea surface temperature variability in the southwest Pacific: A replication study using multiple coral Sr/Ca records from New Caledonia, *Paleoceanography*, 22, PA4212, doi:10.1029/2007PA001444, 2007.
- Dewar, R. E. and Wallis, J. R.: Geographical patterning of inter-annual rainfall variability in the tropics and near tropics: An L-moments approach, *J. Climate*, 12, 3457–3466, 1999.
- Dewar, R. E. and Richard, A. F.: Evolution in the hypervariable environment of Madagascar, *P. Natl. Acad. Sci. USA*, 104, 13723–13727, 2007.
- Douglas, I.: Man, vegetation and the sediment yields of rivers, *Nature*, 215, 925–928, 1967.
- Ersts, P. J. and Rosenbaum, H. C.: Habitat preference reflects social organization of humpback whales (*Megaptera novaeangliae*) on a wintering ground, *J. Zool.*, 260, 337–345, 2003.
- Fallon, S. J., McCulloch, M. T., van Woesik, R., and Sinclair, D.: Corals at their latitudinal limits: Laser ablation trace element systematics in *Porites* from Shirigai Bay, Japan. *Earth Planet. Sci. Lett.*, 172, 221–238, 1999.
- Fallon, S. J., White, J. C., and McCulloch, M. T.: *Porites* corals as recorders of mining and environmental impacts: Misima island, Papua New Guinea, *Geochim. Cosmochim. Ac.*, 66, 45–62, 2002.
- Felis, T., Paetzold, J., and Loya, Y.: Mean oxygen-isotope signatures in *Porites* spp. corals: inter-colony variability and correction for extension-rate effects, *Coral Reefs*, 22, 328–336, 2003.
- Fleitmann, D., Dunbar, R. B., McCulloch, M. T., Mudelsee, M., Vuille, M., McClanahan, T. R., Cole, J. E., and Eggins, S.: East African soil erosion recorded in a 300 year old coral colony from Kenya, *Geophys. Res. Lett.*, 34, L04401, doi:10.1029/2006GL028525, 2007.
- Goodman, S. M. and Benstead, J. P.: The natural history of Madagascar, Univ. of Chicago Press, Chicago and London, 1701, 2003.
- Goodman, S. M. and Ganzhorn, J. U.: Biogeography of lemurs in the humid forests of Madagascar: the role of elevational distribution and rivers. *J. Biogeogr.*, 31, 47–55, 2004.
- Green, G. M. and Sussman, R. W.: Deforestation history of the eastern rain forests of Madagascar from satellite images, *Science*,

- 248, 212–215, 1990.
- Grottoli, A. G.: Effect of light and brine shrimp on skeletal $\delta^{13}\text{C}$ in the Hawaiian coral *Porites compressa*: A tank experiment, *Geochim. Cosmochim. Ac.*, 66, 1955–1967, 2002.
- Grottoli, A. G. and Wellington, G. M.: Effect of light and zooplankton on skeletal $\delta^{13}\text{C}$ values in the eastern Pacific corals *Pavona clavus* and *Pavona gigantea*, *Coral Reefs*, 18, 29–41, 1999.
- Grove, C. A., Nagtegaal R., Zinke, J., Scheufen, T. Koster, B., Kasper, S., McCulloch, M. T., van den Bergh, G., and Brummer, G.-J. A.: River runoff reconstructions from novel spectral luminescence scanning of massive coral skeletons, *Coral Reefs*, 29, 579–591, 2010.
- Hanor, J. S. and Chan, L. H.: Non-Conservative behaviour of barium during mixing of Mississippi River and Gulf of Mexico waters, *Earth. Planet. Sci. Lett.*, 37, 242–250, 1977.
- Harper, G. J., Steininger, M. K., Tucker, C. J., Juhn, D., and Hawkins, F.: Fifty years of deforestation and forest fragmentation in Madagascar, *Environ. Conserv.*, 34, 325–333, 2007.
- Hendy, E. J., Gagan, M. K., and Lough, J. M.: Chronological control of coral records using luminescent lines and evidence for non-stationary ENSO teleconnections in northeast Australia, *The Holocene*, 13, 187–199, 2003.
- Isdale, P.: Fluorescent bands in massive corals record centuries of coastal rainfall, *Nature*, 310, 578–579, 1984.
- Jones, P. D., Briffa, K. R., Osborn, T. J., Lough, J. M., van Ommen, T. D., Vinther, B. M., Luterbacher, J., Wahl, E. R., Zwiers, F. W., Mann, M. E., Schmidt, G. A., Ammann, C. M., Buckley, B. M., Cobb, K. M., Esper, J., Goose, H., Graham, N., Jansen, E., Kiefer, T., Kull, C., Kuttel, M., Mosley-Thompson, E., Overpeck, J. T., Riedwyl, N., Schulz, M., Tudhope, A. W., Villalba, R., Wanner, H., Wolff, E., and Xoplaki, E.: High-resolution paleoclimatology of the last millennium: a review of current status and future prospects, *The Holocene*, 19, 3–49, 2009.
- Juillet-Leclerc, A. and Schmidt, G.: A calibration of the oxygen isotope paleothermometer of coral aragonite from *Porites*, *Geophys. Res. Lett.*, 28, 4135–4138, 2001.
- Jupiter, S., Roff, G., Marion, G., Henderson, M., Schrameyer, V., McCulloch, M., and Hoegh-Guldberg, O.: Linkages between coral assemblages and coral proxies of terrestrial exposure along a cross-shelf gradient on the southern Great Barrier Reef, *Coral Reefs*, 27, 887–903, 2008.
- King, B., McAllister, F., Wolanski, E., Done, T., and Spagnol, S.: River plume dynamics in the central Great Barrier Reef, in: *Oceanographic Processes of Coral Reefs – Physical and biological links in the Great Barrier Reef*, edited by: Wolanski, E., CRC Press, Boca Raton, Florida, 145–159, 2001.
- Kremen, C.: *The natural history of Madagascar: The Masoala Peninsula*, University of Chicago Press, Chicago, 1459–1466, 2003.
- Kremen, C., Razafimahatratra, V., Guillery, R. P., Rakotomalala, J., Weiss, A., and Ratsisompatrarivo, J. S.: Designing the Masoala National Park in Madagascar based on biological and socioeconomic data, *Conserv. Biol. Ser.*, 13, 1055–1068, 1999.
- Larsen, M. C. and Webb, R. M. T.: Potential Effects of Runoff, Fluvial Sediment, and Nutrient Discharges on the Coral Reefs of Puerto Rico, *J. Coast. Res.*, 25, 189–208, 2009.
- Lewis, S. L., Shields, G. A., Kamber, B. S., and Lough, J. M.: A multi-trace element coral record of land-use changes in the Burdekin River catchment, NE Australia, *Palaeogeogr. Palaeoclimatol.*, 246, 471–487, 2007.
- Lewis, S. E., Brodie, J. E., McCulloch, M. T., Mallela, J., Jupiter, S. D., Williams, H. S., Lough, J. M., and Matson, E. G.: An assessment of an environmental gradient using coral geochemical records, Whitsunday Islands, Great Barrier Reef, Australia, *Mar. Pollut. Bull.*, 306–319, doi:10.1016/j.marpolbul.2011.09.030, 2011.
- Linsley, B. K., Wellington, G. M., Schrag, D. P., Ren, L., Salinger, M. J., and Tudhope, A. W.: Geochemical evidence from corals for changes in the amplitude and spatio-temporal pattern of South Pacific interdecadal climate variability over the last 300 years, *Clim. Dynam.*, 22, 1–11, 2004.
- Linsley, B. K., Kaplan, A., Gouriou, Y., Salinger, J., deMenocal, P. B., Wellington, G. M., and Howe, S. S.: Tracking the extent of the South Pacific Convergence Zone since the early 1600s, *Geochem. Geophys. Geosci.*, 7, Q05003, doi:10.1029/2005GC001115, 2006.
- Lough, J. M.: Great Barrier Reef coral luminescence reveals rainfall variability over northeastern Australia since the 17th century, *Paleoceanography*, 26, PA2201, doi:10.1029/2010PA002050, 2011a.
- Lough, J. M.: Measured coral luminescence as a freshwater proxy: comparison with visual indices and a potential age artefact, *Coral Reefs*, 30, 169–182, 2011b.
- Lough, J. M., Barnes, D. J., and McAllister, F. A.: Luminescent lines in corals from the Great Barrier Reef provide spatial and temporal records of reefs affected by land runoff, *Coral Reefs*, 21, 333–343, 2002.
- Maina, J., de Moel, H., Vermaat, J., Bruggemann, H. J., Guillaume, M. M. M., Grove, C. A., Madin, J. S., Mertz-Kraus, R., and Zinke, J.: Linking coral river runoff proxies with climate variability, hydrology and land-use in Madagascar catchments, *Mar. Pollut. Bull.*, doi:10.1016/j.marpolbul.2012.06.027, in press, 2012.
- Marin-Spiotta, E., Swanston, C. W., Torn, M. S., Silver, W. L., and Burton, S. D.: Chemical and mineral control of soil carbon turnover in abandoned tropical pastures, *Geoderma*, 143, 49–62, 2008.
- Matson, E. G.: Core plugs, in: *Encyclopedia of Modern Coral Reefs*, edited by: Hopley, D., Springer, 294–296, 2011.
- McClanahan, T. R. and Obura, D.: Sedimentation effects on shallow coral communities in Kenya, *J. Exp. Mar. Bio. Ecol.*, 209, 103–122, 1997.
- McConnaughey, T.: Sub-equilibrium oxygen-18 and carbon-13 levels in biological carbonates: carbonate and kinetic models, *Coral Reefs*, 22, 316–327, 2003.
- McCulloch, M. T., Gagan, M. K., Mortimer, G. E., Chivas, A. R., and Isdale, P. J. A.: A high-resolution Sr/Ca and $\delta^{18}\text{O}$ coral record from the Great Barrier Reef, Australia, and the 1982–1983 El Niño, *Geochim. Cosmochim. Ac.*, 58, 2747–2754, 1994.
- McCulloch, M. T., Fallon, S., Wyndham, T., Hendy, E., Lough, J., and Barnes, D.: Coral record of increased sediment flux to the inner Great Barrier Reef since European settlement, *Nature*, 421, 727–730, 2003.
- Milliman, J. D. and Syvitski, J. P. M.: Geomorphic tectonic control of sediment discharge to the ocean – The importance of small mountainous rivers, *J. Geol.*, 100, 525–544, 1992.
- Moyer, R. P.: Carbon isotopes ($\delta^{13}\text{C}$ and $\Delta^{14}\text{C}$) and trace elements (Ba, Mn, Y) in small mountainous rivers and coastal coral skeletons in Puerto Rico, Ph.D. thesis, The Ohio State Univ, 2008.

- Moyer, R. P and Grottoli, A. G.: Coral skeletal carbon isotopes ($\delta^{13}\text{C}$ and ΔC) record the delivery of terrestrial carbon to the coastal waters of Puerto Rico, *Coral Reefs*, 30, 791–802, 2011.
- Nagtegaal, R., Grove, C. A., Kasper, S., Zinke, J., Boer, W., and Brummer, G.-J. A.: Spectral luminescence and geochemistry of coral aragonite: Effects of whole-core treatment, *Chem. Geol.*, 318–319, 6–15, 2012.
- Paillard, D., Labeyrie, L., and Yiou, P.: Macintosh program performs time series analysis, *Eos. Trans. AGU*, 77, 379–379, 1996.
- Payet, R. and Obura, D. O.: The negative impacts of human activities in the Eastern African region: An international waters perspective, *Ambio*, 33, 24–33, 2004.
- Pfeiffer, M., Dullo, W. C., Zinke, J., and Garbe-Schönberg, D.: Three monthly coral Sr/Ca records from the Chagos Archipelago covering the period of 1950–1995 A. D.: reproducibility and implications for quantitative reconstructions of sea surface temperature variations, *Int. J. Earth Sci.*, 98, 53–66, 2009.
- Prouty, N. G., Field, M. E., Stock, J. D., Jupiter, S. D., and McCulloch, M.: Coral Ba/Ca records of sediment input to the fringing reef of the southshore of Moloka'i, Hawai'i over the last several decades, *Mar. Pollut. Bull.*, 60, 1822–1835, 2010.
- Quartly, G. D., Kyte, E. A., Srokosz, M. A., and Tsimplis, M. N.: An intercomparison of global oceanic precipitation climatologies, *J. Geophys. Res.*, 112, D10121, doi:10.1029/2006JD007810, 2007.
- Quinn, T. M., Taylor, F. W., Crowley, T. J.: Coral-based climate variability in the Western Pacific Warm Pool since 1867, *J. Geophys. Res.*, 111, C11006, doi:10.1029/2005JC003243, 2006.
- Ren, L., Linsley, B. K., Wellington, G. M., Schrag, D. P., and Hoegh-guldberg, O.: Deconvolving the $\delta^{18}\text{O}$ seawater component from subseasonal coral $\delta^{18}\text{O}$ and Sr/Ca at Rarotonga in the southwestern subtropical Pacific for the period 1726 to 1997, *Geochim. Cosmochim. Ac.*, 67, 1609–1621, 2002.
- Reynaud, S., Ferrier-Pages, C., Sambrotto, R., Juillet-Leclerc, A., Jaubert, J., and Gattuso, J. P.: Effect of feeding on the carbon and oxygen isotopic composition in the tissues and skeleton of the zooxanthellate coral *Stylophora pistillata*, *Mar. Ecol. Prog. Ser.*, 238, 81–89, 2002.
- Reynaud-Vaganay, S., Juillet-Leclerc, A., Jaubert, J., and Gattuso, J. P.: Effect of light on skeletal delta C-13 and delta O-18, and interaction with photosynthesis, respiration and calcification in two zooxanthellate scleractinian corals, *Palaeogeogr. Palaeoclimatol.*, 175, 393–404, 2001.
- Reynolds, R. W., Rayner, N. A., Smith, T. M., Stokes, D. C., and Wang, W.: An improved in situ and satellite SST analysis for climate, *J. Climate*, 15, 1609–1625, 2002.
- Rogers, C. S.: Responses of coral reefs and reef organisms to sedimentation, *Mar. Ecol. Prog. Ser.*, 62, 185–202, 1990.
- Rollion-Bard, C., Chaussidon, M., and France-Lanord, C.: pH control on oxygen isotopic composition of symbiotic corals, *Earth Planet. Sci. Lett.*, 215, 275–288, 2003.
- Sinclair, D. J.: Non-river flood barium signals in the skeletons of corals from coastal Queensland, Australia, *Earth. Planet. Sci. Lett.*, 237, 354–369, 2005.
- Sinclair, D. J. and McCulloch, M. T.: Corals record low mobile barium concentrations in the Burdekin River during the 1974 flood: evidence for limited Ba supply to rivers?, *Palaeogeogr. Palaeoclimatol.*, 214, 155–174, 2004.
- Smith, T. M., Reynolds, R. W., Peterson, T. C., and Lawrimore, J.: Improvements to NOAA's Historical Merged Land-Ocean Surface Temperature Analysis (1880–2006), *J. Climate*, 21, 2283–2296, 2008.
- Smithers, S. G. and Woodroffe, C. D.: Coral microatolls and 20th century sea level in the eastern Indian Ocean, *Earth. Planet. Sci. Lett.*, 191, 173–184, 2001.
- Stecher, H. A. and Kogut, M. B.: Rapid barium removal in the Delaware estuary, *Geochim. Cosmochim. Ac.*, 63, 1003–1012, 1999.
- Swart, P. K., Leder, J. J., Szmant, A. M., and Dodge, R. E.: The origin of variations in the isotopic record of scleractinian corals: II Carbon, *Geochim. Cosmochim. Ac.*, 60, 2871–2885, 1996.
- von Fischer, J. C. and Tieszen, L. L.: Carbon isotope characterization of vegetation and soil organic matter in Subtropical forests in Luquillo, Puerto Rico, *Biotropica*, 27, 138–148, 1995.
- Warrick, J. A. and Rubin, D. M.: Suspended-sediment rating curve response to urbanization and wildfire, Santa Ana River, California, *J. Geophys. Res.*, 112, F02018, doi:10.1029/2006JF000662, 2007.
- Weil, S. M., Buddemeier, R. W., Smith, S. V., and Kroopnick, P. M.: The stable isotopic composition of coral skeletons – Control by environmental variables, *Geochim. Cosmochim. Ac.*, 45, 1147–1153, 1981.
- Windley, B. F., Razafiniparany, A., Razakamanana, T., and Ackermann, D.: Tectonic framework of the Precambrian of Madagascar and its Gondwana connections – a review and reappraisal, *Geol. Rundsch.*, 83, 642–659, 1994.
- Winsemius, H. C., Savenije, H. H. G., Gerrits, A. M. J., Zapreeva, E. A., and Klees, R.: Comparison of two model approaches in the Zambezi river basin with regard to model reliability and identifiability, *Hydrol. Earth Syst. Sci.*, 10, 339–352, doi:10.5194/hess-10-339-2006, 2006.
- Wischmeier, W. H. and Smith, D. D.: Predicting rainfall erosion losses – a guide to conservation planning, U.S. Department of Agriculture, Washington DC, AH-537, 1978.
- Xie, P. P. and Arkin, P. A.: Analyses of global monthly precipitation using gauge observations, satellite estimates, and numerical model predictions, *J. Climate*, 9, 840–858, 1996.
- Zinke, J., Pfeiffer, M., Timm, O., Dullo, W. C., Kroon, D., and Thomassin, B. A.: Mayotte coral reveals hydrological changes in the western Indian Ocean between 1881 and 1994, *Geophys. Res. Lett.*, 35, L23707, doi:10.1029/2008GL035634, 2008.